Regulation of the Dimerization and Activity of SARS-CoV-2 Main Protease through Reversible Glutathionylation of Cysteine 300

David A. Davis[1], Haydar Bulut[1], Prabha Shrestha[1], Amulya Yaparla[1], Hannah K. Jaeger[1], Shin-ichiro Hattori[3], Paul T. Wingfield[2], Hiroaki Mitsuya[1,3], and Robert Yarchoan*[1]

[1]*HIV and AIDS Malignancy Branch, Center for Cancer Research, National Cancer Institute, Bethesda, MD 20892.* [2]*National Institute of Arthritis and Musculoskeletal and Skin Diseases, National Institutes of Health, Bethesda, MD 20892*

[3]*Department of Refractory Viral Infections, National Center for Global Health and Medicine Research Institute, Tokyo, Japan*

*Corresponding Author: Robert Yarchoan: robert.yarchoan@nih.gov

Abstract

SARS-CoV-2 encodes main protease (M^{pro}), an attractive target for therapeutic interventions. We show M^{pro} is susceptible to glutathionylation leading to inhibition of dimerization and activity. Activity of glutathionylated M^{pro} could be restored with reducing agents or glutaredoxin. Analytical studies demonstrated that glutathionylated M^{pro} primarily exists as a monomer and that a single modification with glutathione is sufficient to block dimerization and loss of activity. Proteolytic digestions of M^{pro} revealed Cys300 as a primary target of glutathionylation, and experiments using a C300S M^{pro} mutant revealed that Cys300 is required for inhibition of activity upon M^{pro} glutathionylation. These findings indicate that M^{pro} dimerization and activity can be regulated through reversible glutathionylation of Cys300 and provides a novel target for the development of agents to block Mpro dimerization and activity. This feature of M^{pro} may have relevance to human disease and the pathophysiology of SARS-CoV-2 in bats, which develop oxidative stress during flight.

53 **Main Text**

54 **INTRODUCTION**

55 The main protease (M^{pro}) of SARS-CoV-2 coronavirus is encoded as part of two large
56 polyproteins, pp1a and pp1ab, and is responsible for at least 11 different cleavages. Thus, M^{pro} is essential
57 for viral replication and has been identified as a promising target for the development of therapeutics for
58 treatment of coronavirus disease 2019 (COVID-19) [1, 2]. M^{pro} is known as a 3C-like protease (3CL) due to
59 its similarity to picornavirus 3C protease in its cleavage site specificity [3]. Through extensive studies on
60 M^{pro} from SARS-CoV-1, whose sequence is 96% identical to SARS-CoV-2 M^{pro}, a wealth of information
61 has been obtained that can be applied to studies now ongoing with SARS-CoV-2 M^{pro} (for review see [4]).
62 M^{pro} of SARS-CoV-1 and SARS-CoV-2 consist of three major domains, I, II, and III. Unlike other 3C-like
63 proteases, studies on M^{pro} from SARS-CoV-1 and SARS-CoV-2 have revealed that they are only active as
64 homodimers even though each individual monomeric subunit contains its own active site [5, 6]. Studies on
65 SARS-CoV-1 to explain why dimerization is required for activity have revealed that, in the monomeric
66 state, the active site pocket collapses and is not available for substrate binding and processing [7]. In these
67 studies it was also revealed that the extra domain (III) plays a key role in dimerization and activation of
68 M^{pro} and that arginine 298 in this domain is essential to allow proper dimerization and M^{pro} activity [7].

69 The proteases of HIV and other retroviruses are also active as homodimers, and we previously
70 demonstrated that each of the retroviral proteases studied (HIV-1, HIV-2 and HTLV-1) could be
71 reversibly regulated through oxidation of residues involved in protease dimerization [8, 9, 10, 11]. The activity
72 of HIV-1 and HIV-2 protease can be reversibly inhibited by oxidation of residue 95, located at the dimer
73 interface [9] and these oxidative modifications are reversible with cellular enzymes, glutaredoxin (Grx)
74 and/or methionine sulfoxide reductase, respectively [12, 13]. The majority of other retroviral proteases also
75 have one or more cysteine and/or methionine residues at the dimer interface region and modification of
76 these residues, under conditions of oxidative stress, would be predicted to similarly regulate dimerization
77 and activity [8]. There is further evidence that HIV polyprotein precursors encoding these proteases are
78 initially formed in an oxidized inactive state and need to be activated in a reducing environment [8, 9, 13, 14,

79 [15]. Moreover, the initial step in HIV-1 polyprotein processing, which is required to release the mature
80 protease, is also regulated through reversible oxidation of cysteine 95 [16].
81 In addition to the active site cysteine, M^{pro} of SARS-CoV-1 and SARS-CoV-2 contain 11 other
82 cysteine residues throughout the 306 amino acid sequence and all these residues are present in their
83 reduced form in the crystal structures of M^{pro}. This is a relatively large number of cysteines for a protein
84 of this size (3.9% vs 2.3% average cysteine content of human proteins) [17]. While a number of the
85 cysteines are buried and may not be exceptionally susceptible to oxidation in the native structure, there
86 are certain cysteine residues (notably cysteine 22, 85, 145, 156 and 300) that are at least partially
87 surface/solvent exposed and potentially susceptible to oxidative modification. Here, we demonstrate that
88 dimerization and activity of SARS-CoV-2 M^{pro} can be regulated through reversible glutathionylation of
89 cysteine 300.
90
91 **RESULTS**
92 **Treatment of M^{pro} with oxidized glutathione inhibits protease activity**
93 M^{pro} activity was measured utilizing a para nitroanilide (pNA) substrate (H2N-TSAVLQ-pNA) as
94 described previously for SARS-CoV-1 M^{pro} [18]. To assess the effects of oxidized glutathione (GSSG) and
95 reduced glutathione (GSH) on M^{pro}, we treated M^{pro} at concentrations of either 1.2 or 18 μM with 2 mM or
96 10 mM of GSSG or GSH for 30 minutes at 37ºC and then measured activity. Previous reports have indicated
97 that the K_d of M^{pro} dimerization is about 2 μM [6] and that is consistent to what we found in this work. Thus,
98 M^{pro} would be predicted to be largely monomeric at 1.2 μM and dimeric at 18 μM. After exposure of 1.2
99 μM M^{pro} to 2 mM GSSG, activity was inhibited by an average of 44% while after exposure to 10 mM GSSG,
100 activity was inhibited by more than 90% (Figure 1A). By contrast, GSH had little effect or somewhat
101 increased protease activity at these concentrations (Figure 1A). Interestingly, when the M^{pro} concentration
102 was increased to 18 μM it was largely resistant to GSSG inhibition, with no inhibition observed with 2 mM
103 GSSG and less than 20% inhibition with 10 mM GSSG (Figure 1B). These results suggest that monomeric
104 M^{pro} may be more sensitive to glutathionylation than dimeric M^{pro}. To confirm that M^{pro} was becoming

105 modified with glutathione under these conditions, we acidified the samples at the end of the enzyme assays
106 with formic acid/trifluoroacetic acid (FA/TFA) to arrest activity and glutathionylation and analyzed them
107 by RP-HPLC/MALDI-TOF. The extent of glutathionylation was assessed by determining the mass of M^{pro}
108 by protein deconvolution and by looking for the addition of approximately 305 amu and/or multiples of
109 305 to M^{pro} consistent with the addition of glutathione(s) via a disulfide bond. As revealed by RP-
110 HPLC/MALDI-TOF analysis, treatment of 1.2 μM M^{pro} with 2 mM GSSG led to an estimated 45%
111 monoglutathionylation (only an estimate based on the mass abundances), whereas treatment with 10 mM
112 GSSG led to mono- (11%), di- (50%), and tri-glutathionylation (35%), with less than 4% of M^{pro} remaining
113 unmodified (Figure 1C). Comparing the results of Figure 1A and 1C, the loss of M^{pro} activity correlated
114 with the extent of glutathionylation. Interestingly, the data obtained with 2 mM GSSG suggested that
115 modification of only one cysteine may be sufficient to lead to inhibition of M^{pro} activity, as this treatment
116 yielded about 45% monoglutathionylation and showed an average 40% decrease in activity. By contrast,
117 M^{pro} incubated at 18 μM during treatment with 2 mM GSSG showed very little modification or reduction
118 in activity (Figures 1B and 1D). Moreover, treatment of 18 μM M^{pro} with 10 mM GSSG led to only 14%
119 monoglutathionylation (Figure 1D), which was associated with an average inhibition of 18% (Figure1B).
120

121 **Inhibition of M^{pro} activity by glutathionylation is reversible**

122 To better understand the nature of M^{pro} inhibition by glutathionylation, we modified M^{pro} with 10
123 mM GSSG at pH 7.5, as described in the Materials and Methods, so that nearly all the M^{pro} was modified
124 with at least one glutathione. Excess GSSG was removed by washing through an Amicon 10 kDa cut-off
125 membrane. RP/HPLC//MALDI-TOF analysis of this preparation on a C18 column followed by protein
126 deconvolution indicated M^{pro} was now a mixture of mono (23%), di (68%) and triglutathionylated forms
127 (9%) with little detectable unmodified M^{pro} (based on abundances form protein deconvolution) (Figure 2A).
128 To determine if the modification was reversible with thiol reducing agents, we treated the glutathionylated
129 preparation with 10 mM DTT for 30 minutes. This resulted in more than 90% of the glutathionylated M^{pro}
130 being converted back to native M^{pro} (Figure 2B). We then tested the activity of glutathionylated M^{pro}.

131 Glutathionylated M^{pro} had less than 5% of the activity of unmodified M^{pro}, confirming that glutathionylation
132 was inhibiting protease activity (Figure 2C). Following the addition of 10 mM DTT, the activity was fully
133 restored, while DTT marginally improved native M^{pro} activity (Figure 2C).
134
135 **Glutathionylation of M^{pro} inhibits M^{pro} dimerization**
136 To assess M^{pro} dimerization we established a method consisting of size exclusion chromatography
137 (SEC) coupled to mass spectrometry similar to that described previously for HIV-1 protease [14]. In the SEC
138 experiments we initially used SEC3000 columns and later SEC2000 columns from Phenomenex, both
139 which could be used successfully to separate M^{pro}. When injected at 60 μM on a SEC3000 column,
140 unmodified M^{pro} eluted at 8.8 minutes (Figure 3A, black tracing) while glutathionylated M^{pro} eluted at 9.2
141 minutes (Figure 3A, red tracing). Protein deconvolution of the eluting M^{pro} confirmed the expected mass
142 for unmodified M^{pro} (Figure 3B, black) and the glutathionylated forms of M^{pro} (Figure 3C, red). However,
143 when injected at 7.5 μM, unmodified M^{pro} clearly eluted as two peaks at 8.9 and 9.4 minutes (Figure 3D,
144 black tracing), while the glutathionylated M^{pro} still predominantly eluted at the later retention time (9.4
145 minutes) (Figure 3D, red tracing). Again, the masses for native and glutathionylated M^{pro} were confirmed
146 (Figure 3E black tracing and 3F red tracing, respectively). Thus, the unmodified M^{pro} appeared to behave
147 as a typical monomer/dimer two-species system with dimerization dependent on concentration, while
148 glutathionylated M^{pro} behaved essentially as a single monomer-like species independent of its concentration.
149 We carried out equilibrium analytical ultracentrifugation (AUC) on M^{pro} and glutathionylated M^{pro} to obtain
150 both the molecular mass of the species and the K_d for dimerization. Matched native and glutathionylated
151 M^{pro} samples (18 μM) were analyzed by AUC. The results indicated that native M^{pro} was in equilibrium
152 between monomeric and dimeric forms and behaved with a calculated dimerization K_d of 2.4 μM (Figure
153 3G); consistent with previous reports [6]. At high concentrations (60 μM), it was almost completely dimeric.
154 By contrast, under the same conditions, the glutathionylated M^{pro} behaved almost completely monomeric
155 with an estimated K_d of 200 μM (Figure 3H), indicating that glutathionylation was inhibiting dimerization
156 of M^{pro}.

157

158 **Modification of a single cysteine of M^{pro} leads to inhibition of dimerization and activity**

159 To determine if glutathionylation of a single cysteine might render the enzyme monomeric and
160 inactive, we generated a glutathionylated M^{pro} preparation by exposing 1.2 μM M^{pro} to 5 mM GSSG at pH
161 6.8, a pH that would favor the glutathionylation of only the most reactive cysteines (with low pKa's). This
162 monoglutathionylated preparation was run on SEC at 8 μM and ran as two peaks indicating the existence
163 of both dimeric and monomeric forms of M^{pro} (Figure 4A). Deconvolution of these two peaks revealed both
164 native and monoglutathionylated M^{pro} as expected and contained an estimated 35% monoglutathionylated
165 M^{pro} and less than 5% diglutathionylated M^{pro}, with the remaining M^{pro} unmodified (Figure 4B). However,
166 while the mass of the unmodified M^{pro} was detected in both peaks since it is present in both monomeric and
167 noncovalent dimeric forms (Figure 4C), the mass corresponding to monoglutathionylated protease was
168 detected predominantly (>70% of the total area) in the second peak (Figure 4D). Treatment of the
169 glutathionylated M^{pro} with reducing agent TCEP resulted in a decrease in the second monomeric peak
170 (Figure 4E) and complete conversion to native M^{pro} (Figure 4F) with an elution profile consistent with
171 native M^{pro} (Figure 4G). We also collected the first and second peaks eluting from SEC analysis of the
172 monoglutathionylated preparation as seen in Figure 4A (peaks 1 and 2 labeled in Figure 4A) and tested
173 them for M^{pro} activity. In the absence of 50 mM TCEP, the activity of the second peak was only 25% of
174 that of the first peak ($P<0.005$) (Figure 4H). In the presence of TCEP, activity of the second peak increased
175 significantly ($P<0.01$) while having no significant effect on the first peak (Figure 4H). These data provide
176 strong evidence that monoglutathionylated M^{pro} behaves as a monomer, is inactive, and that these effects
177 are reversible.

178

179 **Inhibition of M^{pro} activity by glutathionylation is reversible with glutaredoxin (Grx)**

180 Grx (also known as thioltransferase) is a ubiquitous cellular enzyme that is able to reverse
181 glutathionylation of a number of different cellular proteins including hemoglobin, nuclear factor-1, PTP1B,
182 actin, Ras, IκB kinase, procaspase 3, and IRF-3, as well as viral proteins including HIV-1-protease and

183 HTLV-1 protease [19, 20]. We tested whether Grx could deglutathionylate M^{pro} and restore its activity.
184 Preparations of glutathionylated M^{pro} were prepared at pH 7.5 or pH 6.8 and then tested for reversibility of
185 glutathionylation and restoration of activity following treatment with Grx. The glutathionylated preparation
186 made at pH 7.5 contained no detectable unmodified M^{pro} and was predominantly diglutathionylated M^{pro}
187 (75%) and monoglutathionylated (22%) with the remainder triglutathionylated (3%) (Figure 5A).
188 Incubation of the preparation with 350 nm GSH alone, a cofactor required for Grx activity, produced a
189 small amount of detectable unmodified M^{pro} (1.5%) but led to only minor changes in the percentages of the
190 other forms of M^{pro} (Figure 5B). However, incubation of glutathionylated M^{pro} with Grx in the presence of
191 0.5 mM GSH resulted in the loss of the triglutathionylated M^{pro}, a substantial decrease in the
192 diglutathionylated M^{pro} (from 75% to 16%), an increase in monoglutathionylated M^{pro} (22% to 65%) and
193 the production of native M^{pro} which made up 19% of the total M^{pro} (Figure 5C). M^{pro} activity was then
194 assessed under these same conditions. Incubation of glutathionylated M^{pro} with 350 nM Grx in the presence
195 of 0.5 mM GSH led to a significant increase in protease activity, restoring an average 58% of the activity
196 compared to untreated M^{pro}, while 0.5 mM GSH alone restored only about 10% of the activity (Figure 5D).
197 We also assessed the ability of Grx to deglutathionylate the preparation made at pH 6.8. The
198 glutathionylated preparation made at pH 6.8 contained approximately 30% monoglutathionylated M^{pro}
199 based on percent abundance, and less than 2% diglutathionylated with the remainder (68%) being
200 unmodified (Figure 5E). Incubation of this preparation with GSH alone for 30 min again led to insignificant
201 changes in the percentages of monoglutathionylated M^{pro} (69.3% native, 2.9% monoglutathionylated and
202 1.7% diglutathionylated) (Figure 5F). However, incubation of this preparation of M^{pro} with 350 nm Grx in
203 the presence of GSH resulted in loss of the diglutathionylated M^{pro} and a decrease in the percentage of
204 monoglutathionylated M^{pro}, going from an average 29% to 14% monoglutathionylated M^{pro} with a
205 corresponding increase (from 69% to 86%) in unmodified M^{pro} (Figure 5G). Furthermore, Grx was found
206 to reverse glutathionylation of M^{pro} as assessed by SEC-MALDI-TOF and restore activity in a dose
207 dependent manner (Figure 5H), and at 175 nM, Grx restored 100% of the activity (Figure 5I). Interestingly,
208 even at the highest concentration of Grx tested (350 nM), about 14% of the M^{pro} remained in a

209 monoglutathionylated form (Fig 5H). This suggests that Grx is preferentially removing glutathione from
210 cysteines whose glutathionylation is responsible for inhibition of activity while sparing certain cysteines
211 whose modification does not alter activity.
212
213 **Identification of glutathionylated cysteines by MALDI-TOF MS**
214 To determine which cysteines of M^{pro} might be primarily responsible for the inhibition of
215 dimerization and activity, we digested native M^{pro} and a monoglutathionylated preparation of M^{pro}
216 (containing approximately 35% monoglutathionylated forms of M^{pro}) with either chymotrypsin or a
217 combination of trypsin and lysC to produce peptides that could be assessed for glutathionylation. Prior to
218 digestion, we alkylated the free cysteines in the M^{pro} preparations with N-ethylmaleimide (NEM) using the
219 AccuMAP™ System (Promega); this step limits disulfide scrambling during the alkylation and proteolytic
220 digestion processes. For digestions of native M^{pro} (see Figure S2A for TIC chromatogram and S2B for UV
221 chromatogram in supplemental material) that was fully alkylated with NEM, we were able to identify
222 alkylated peptides for 7 of the 12 cysteines of M^{pro} including cysteines 38, 44, 117, 128, 145, 156 and 300
223 by using molecular ion extraction for the predicted monoisotopic masses (see peptides 1-10 in Table S1 in
224 supplemental material) along with 12 other non-cysteine containing peptides (see peptides 15-27 in Table
225 S1 in supplemental material). To identify which cysteines were becoming glutathionylated in the
226 glutathionylated M^{pro} preparation (see Figure S2C for TIC chromatogram and S2D for UV chromatogram
227 in supplemental material), we searched for the predicted glutathionylated monoisotopic masses by
228 molecular ion extraction of the TIC chromatogram obtained from RP-HPLC/MALDI-TOF analysis of
229 chymotrypsin digests. We located monoisotopic masses consistent with that for three glutathionylated
230 peptides (glutathione adds a net 305.08 amu): peptides ^{151}NIDYDC^{GSH}VSF^{159}, ^{295}DVVRQC^{GSH}SGVTF^{305}
231 and ^{295}DVVRQC^{GSH}SGVTFQ^{306} with glutathionylated Cys^{156,} Cys^{300}, and Cys^{300}, respectively (Table 1 and
232 see Figure S3A-S3J for detailed analysis in supplemental material). All three of these peptides had
233 experimental masses that were within 0.04 amu of the predicted glutathionylated masses (predicted
234 monoisotopic mass increase with glutathione is 305.08) consistent with addition of glutathione. To confirm

235 that these peptides were, indeed, glutathionylated forms of the predicted M^{pro} peptides, we analyzed the
236 peptide digests both before and after treating them with TCEP to reduce any disulfide bonds (see Figure
237 S2E for TIC chromatograms and S2F for UV chromatograms in supplemental material). When this was
238 done, the masses for all three of the predicted glutathionylated peptides were no longer detected, due to the
239 removal of glutathione with TCEP, and in place we were able to locate the predicted native masses expected
240 following removal of glutathione for all three peptides (Table 1 and see Figure S3K-S3P in supplemental
241 material). The difference (Delta) between the experimental and calculated masses was less than 0.05 amu
242 for all peptides providing strong confidence in their identity (Table 1).

243 Due to the inability to assess modification of cysteines 16, 22, 85, 161 and 265 using the
244 chymotrypsin data, as the peptides carrying these residues were not located (see Table S1 for a list of the
245 peptides found in supplemental material), we prepared trypsin/lysC digests of native M^{pro} and the same
246 monoglutathionylated M^{pro} preparation used in the chymotrypsin experiments (see Figure S4A,C for TIC
247 chromatogram and S5B,D for UV chromatograms). Interrogation of the TIC chromatogram for masses
248 corresponding to glutathionylated forms of cysteine-containing peptides revealed masses consistent with
249 glutathionylation of three peptides: ^{77}VIGHSMQNC^{GSH}VLK^{88}, ^{299}QC^{GSH}SGVTFQ^{306} and
250 ^{299}pyQC^{GSH}SGVTFQ^{306} (the pyroglutamate (py) form of the 299-306 peptide that results from spontaneous
251 deamidation of peptides with N-terminal glutamyl residues[21]) (Table 2 and see Figure S5A-S5J in
252 supplemental material). These were glutathionylated at Cys^{85}, Cys^{300}, and Cys^{300}, respectively. All three
253 peptides had experimental masses within 0.04 amu of the predicted calculated glutathionylated masses
254 consistent with glutathione modification (Table 2). Also, the calculated masses for the three native forms
255 were found following analysis of the tryptic digests after reduction with TCEP (Table 2 and see Figure
256 S5E-S5P in supplemental material). The difference (Delta) between the experimental and calculated masses
257 was less than 0.05 amu providing strong confidence in their identity (Table 2). The data from the
258 trypsin/lysC digestion indicated that the majority of the monoglutathionylation was occurring at Cys300.
259 We based this on the greater area at 205 nm obtained for glutathionylated Cys300 peptides than the cys85
260 peptide (combined area for glutathionylated cys300 peptides at 205 nm was 301 vs 56 for the

261 glutathionylated cys85 peptide) and their native forms (combined area at 205 nm for native cys300 peptides
262 was 272 vs 21 for the native cys85 peptide) (see Figure S5C-S5D in supplemental material). Taken together,
263 the data obtained from the chymotryptic and tryptic/lysC digestions of M^{pro} and glutathionylated M^{pro}
264 strongly implicated Cys300 as a primary target for glutathionylation. Given the location of Cys300 near the
265 dimer interface and the importance of amino acids 298 and 299 for dimerization [4, 7] we hypothesized that
266 glutathionylation of this cysteine is likely responsible for interfering with dimerization leading to inhibition
267 of M^{pro} activity.
268
269 **Cys300 is required for inhibition of M^{pro} activity following glutathionylation**
270 To determine if Cys300 was contributing to the inhibition of activity of M^{pro} following
271 glutathionylation, we prepared a C300S mutant M^{pro} (for purity and molecular weight analysis see Figure
272 S1F-S1I) and evaluated the effects of glutathionylation on M^{pro} activity. We treated WT and C300S M^{pro} at
273 1.2 μM with 10 mM GSSG for 30 minutes and then measured activity. In these experiments, the activity of
274 WT M^{pro} was inhibited by more than 50% while C300S M^{pro} was not significantly affected (Figure 6A). We
275 also measured the extent of glutathionylation for WT and C300S M^{pro} following the enzyme assay. Based
276 on the absolute abundances of each form, we found that WT M^{pro} had 46%, 14% and 5% mono, di and
277 triglutathionylated forms, respectively, with the remainder (35%) unmodified while after the same
278 treatment, C300S had 36% and 11% mono and diglutathionylated forms, respectively, with the remainder
279 (53%) unmodified (see Figure S6A-S6D in supplemental material). This indicated that while almost 50%
280 of C300S could still become glutathionylated at other cysteine residues, its activity was unaffected, strongly
281 implicating Cys300 in the inhibition of M^{pro} activity following glutathionylation of WT M^{pro}. To determine
282 if Cys300 was the primary target for glutathionylation when incubating with GSSG at the lower pH of 6.8,
283 we treated WT and C300S M^{pro} with 5 mM GSSG at pH 6.8 for 2.5 hours to produce monoglutathionylated
284 forms of M^{pro}. Based on SEC/MALDI-TOF analysis the WT M^{pro} was 36% glutathionylated while the
285 C300S M^{pro} was only 16% glutathionylated based on the abundances for each form (supplemental Figure
286 S6E-S6F). This data suggests that there are at least two reactive cysteines under these lower pH conditions.

287 Activity of these preparations was measured before and after reduction with DTT. DTT increased the
288 activity of the monoglutathionylated WT M^{pro} preparation by 26% but had no significant effect on the
289 activity of monoglutathionylated C300S M^{pro} mutant (Figure 6B). This suggests that while the C300S
290 mutant can still become glutathionylated at alternative cysteines, the modification has little effect on M^{pro}
291 activity.
292
293 **Discussion**
294 In cells that are under oxidative stress, cellular and foreign proteins can undergo glutathionylation,
295 and this process, which is reversible, can alter the function of these proteins [18, 19, 22, 23, 24]. Biochemical studies
296 with GSSG can be carried out to determine if reversible glutathionylation might regulate the activity of key
297 proteins although glutathionylation of proteins within cells more likely goes through sulfenic acid
298 intermediates[19]. In this study, we show that glutathionylation of SARS-CoV-2 M^{pro} inhibits M^{pro} activity,
299 and this is reversible with reducing agents or the ubiquitous cellular enzyme, Grx. We also show that loss
300 of activity is due to inhibition of M^{pro} dimerization following modification of Cys300. Cys300 of M^{pro} is
301 located proximal to Arg298 and Gln299, both of which play pivotal roles in M^{pro} dimerization in the C-
302 terminal dimerization domain [4]. Our data indicate Cys300 is particularly sensitive to glutathionylation, as
303 we were able to modify Cys300 at pH 6.8, a pH where cysteines are usually protonated and unreactive due
304 to typical pKa's around pH 8. Our current model for regulation of dimerization and activity of M^{pro} is shown
305 in Figure 7A. Our data indicates that monomeric M^{pro} is susceptible to glutathionylation at Cys300 and this
306 blocks dimerization. Grx can reverse the modification, thus restoring dimerization and activity of M^{pro}
307 (Figure 7A). We hypothesize that glutathionylation of Cys300 in SARS-CoV-2 infected cells would inhibit
308 M^{pro} activity and therefore decrease SARS-CoV-2 replication during oxidative stress. Thus, SARS-CoV-2
309 M^{pro}, and by analogy SARS-CoV-1, are quite similar to retroviral proteases in being essential for viral
310 replication, requiring dimerization for activity, and being susceptible to reversible inhibition by
311 glutathionylation [8, 9, 11, 13, 14, 15, 16].

312 Identification of which cysteines in SARS-CoV-2 M^{pro} are glutathionylated was not a trivial matter
313 as M^{pro} contains 12 cysteine residues all in their reduced form. For this reason, we used the Accumap™ low
314 pH system to alkylate M^{pro} with NEM to minimize disulfide scrambling during the reactions. Our studies
315 indicated that at least two cysteines were readily modified by GSSG including Cys300 and Cys156 (Figure
316 7B). We identified glutathionylated peptides by their predicted monoisotopic masses and the alkylated
317 forms of these peptides in controls using RP/HPLC/MALDI-TOF, and also showed the disappearance of
318 these masses after reduction with TCEP leading to the appearance of their native peptide counterparts. The
319 identity of Cys300 glutathionylated and native and alkylated peptides were further confirmed with the use
320 of synthetic peptides used as standards to determine masses and retention times. The data from
321 chymotryptic and tryptic/lysC digestions implicated Cys300; therefore, we prepared a C300S M^{pro} mutant
322 to verify the role of cysteine Cys300 in inhibition by glutathionylation. Indeed, C300S M^{pro} was no longer
323 susceptible to inhibition by glutathionylation under the same conditions where WT M^{pro} was, thus
324 confirming the role for Cys300 in this process.

325 Glutathionylation of proteins occurs via a mixed disulfide between glutathione and a cysteine
326 residue. Most cysteine residues have relatively high pKa's (pH 8.0 or greater) and usually remain protonated
327 under physiologic conditions, making them relatively unreactive at typical cellular pH. However, studies
328 have shown that the local environment around certain cysteine residues can lower their pKa making them
329 more susceptible to oxidation and glutathionylation [25, 26, 27]. We propose that the local environment of
330 Cys300 may account for this particular susceptibility to glutathionylation. Previous studies have found that
331 the presence of basic residues or serine hydroxyl sidechains in the local environment can substantially
332 reduce the pKa of the thiol sidechain [25, 28]. As to Cys300, there is a basic residue at Arg298 and a hydroxyl
333 residue at Ser301. This may increase the local acidity of the Cys300 thiol group in the monomer making it
334 more prone to oxidation while in the dimeric state Arg298 is involved in interactions which stabilize the
335 dimer [7]. In the SARS-CoV-2 dimer Inspection of a previously determined monomeric form of SARS-CoV-
336 1 M^{pro} (R298A) reveals that the carbonyl sidechains of Asn214 and Gln299, which can act as hydrogen
337 acceptors and potentially destabilize the thiol group, have close contact with the Cys300 thiol (Figure 8).

338 Although there is not a monomer structure of SARS-CoV-2 M^{pro} the distances of the Cys300 thiol to the
339 carbonyls in SARS-CoV-1 and 2 is much greater, possibly decreasing its reactivity (see Figure S7A and
340 S7B in supplemental material).

341 It is possible that regulation of M^{pro} through reversible oxidation/glutathionylation of M^{pro} may have
342 evolved in part as a mechanism to blunt viral processing and replication in cells undergoing significant
343 oxidative stress which otherwise may generate defective viral particles. It's known that viral infection itself
344 leads to oxidative stress in cells even early on in infection [29]. In the case with SARS-CoV-2, Cys300 may
345 act as a sensor to regulate when viral proteolytic processing should take place to optimize the generation of
346 new virions. Moreover, M^{pro} from SARS-CoV-1 and SARS-CoV-2 contain 12 cysteines and 10 methionine
347 residues. Studies have shown that such residues can act as decoys to prevent permanent damage to proteins
348 during oxidative stress [30, 31]. In the case of M^{pro}, this could help protect the active site cysteine required for
349 catalysis. It should be noted that the details of the initial autocatalytic processing of M^{pro} from the
350 polyprotein pp1a and pp1ab are still not fully understood, but in the case of HIV, we have shown that similar
351 modifications can also affect the initial autocleavage of the Gag-Pol-Pro polyprotein [11, 16].

352 Another possible factor that may have led to this feature of coronavirus M^{pro} relates to its evolution
353 in bats. It's important to point out that the M^{pro}'s from the three closest relatives to SARS-CoV-2 derived
354 from bats [32] have an extremely high degree of amino acid identity (see Figure S8 in supplemental material)
355 to that of SARS-CoV-2 and all three contain 12 cysteine residues including Cys300. SARS-CoV-2 is
356 thought to have jumped to humans from an original reservoir in *Rhinolophus* bats, possibly through an
357 intermediate host [33]. Bats are reservoirs for a vast number of coronaviruses and other RNA viruses and are
358 often infected with these viruses without showing any signs of disease [34]. One reason for this coexistence
359 is that bats have evolved an immune response to RNA viruses with substantial interferon activity but a
360 minimal inflammatory response [34]. The act of flying requires considerable metabolic energy, and when in
361 flight and during migration, bats are placed under high levels of oxidative stress [35, 36, 37]. Moreover, bats
362 spend much of their lives in densely populated shelters such as caves that facilitate virus transmission.
363 Maintaining the health of host bat colonies would appear to be a good evolutionary strategy for

364 coronaviruses and one can speculate that SARS-CoV-1 and SARS-CoV-2 and related RNA bat viruses
365 have co-evolved so as to persist in bat colonies by not killing off their host animals. Part of this evolutionary
366 adaption might be dampening of viral replication under conditions of oxidative stress, through the inhibition
367 of M^{pro} by glutathionylation. At this time, it is unclear what ramifications these effects from M^{pro}
368 glutathionylation might have for SARS-CoV-2 infection in humans. Unlike bats, humans are not exposed
369 to the metabolic and oxidative stress that is encountered in bats during flight and therefore would not be
370 expected to suppress SARS-CoV-2 replication through this mechanism. This may help explain the
371 relatively more severe manifestations of SARS-CoV-2 infection in humans than in bats.

372 A more practical implication of our findings is that it can inform the development of anti-viral
373 drugs against SARS-CoV-2. While vaccines are effective at preventing COVID-19, effective anti-SARS-
374 CoV-2 drugs are urgently needed and will be in the foreseeable future. Because of its essential role in
375 SARS-CoV-2 replication, M^{pro} is an attractive target for drug development. Nearly all of this effort has
376 focused on active site inhibitors of M^{pro} which can block SARS-CoV-2 replication and cytopathic effect [1,
377 2, 6 38]. Our observation that Cys300 at the dimer interface is particularly susceptible to oxidative modification,
378 and that this modification can block dimerization of M^{pro} resulting in inhibition of activity, demonstrates an
379 alternative way of targeting M^{pro}. Being on the M^{pro} surface in the monomer, this cysteine may be highly
380 accessible and may thus be a promising target for the development of specific M^{pro} inhibitors. In this regard,
381 Gunther and Reinke et al.[38] have recently identified the hydrophobic pocket consisting of Ile21, Leu253,
382 Gln256, Val297, and Cys300 of SARS-Cov-2 Mpro as an allosteric binding site for non-active site M^{pro}
383 inhibitors. Our results indicate that this area can be specifically targeted through Cys300, which is highly
384 reactive and leads to inhibition of dimerization.
385
386
387
388
389

390 **Materials and Methods**

391 ***Enzymes, peptides and reagents***

392 The substrate peptide for M^{pro} (H2N-TSAVLQ-pNA) and peptides corresponding to some of the
393 predicted chymotryptic fragments containing cysteine residues including M^{pro} peptide fragments 113:118,
394 127:134, 141:150, 155:159, 295: 305 and 295: 306 as well the predicted tryptic fragment, 299:306, were
395 obtained (>95% purity) from New England Peptide (Gardner, MA). Amicon Ultra- Centrifugal Filters (10
396 kDa cutoff, 0.5 ml and 15 ml), carboxymethyl bovine serum albumin (cm-BSA), oxidized and reduced
397 forms of L-glutathione (Bioxtra) (>98%), 4-nitroaniline (>99%), the reducing agents Tris (2-carboxyethyl)
398 phosphine hydrochloride (TCEP) and dithiothreitol (DTT) were from Sigma-Aldrich (Milwaukee, WI).
399 BioSep SEC3000 and SEC2000 size exclusion columns (300 x 4.6 mm) were from Phenomenex (Torrence,
400 CA). The VydacC18 column (218TP5205) was from MAC-MOD Analytical (Chadds Ford, PA). Peptide
401 desalting columns from ThermoFisher Scientific (Pittsburgh, PA) and AccuMap™ low pH protein
402 digestion kit (with trypsin and lysC) and chymotrypsin (sequencing grade) were from Promega (Madison,
403 WI). PreScisson protease was from GenScript (Piscataway, NJ). Recombinant human glutaredoxin (Grx)
404 transcript variant 1 was from Origene (cat# TP319385) (Rockville, MD) and stored at -70ºC in 25 mM
405 Tris.-HCl, pH 7.3, 100 mM glycine and 10% glycerol (7 µM stock).

406

407 ***Expression and purification of Authentic M^{pro} and C300S M^{pro}***

408 The SARS-CoV2 M^{pro}-encoding sequence and C300S mutant sequence were cloned into pGEX-
409 4T1 vector (Genscript) with N-terminal self-cleavage site (SAVLQ/SGFRK) and C-terminal His_6-tag as
410 previously designed by others [6]. The plasmid constructs were transformed into BL21 Star™ (DE3) cells
411 (Thermo Fisher Scientific). The cultures were grown in Terrific Broth media supplemented with ampicillin
412 (Quality Biological, Gaithersburg, MD). Protein expression was induced by adding 1 mM iso-propyl b-D-
413 thiogalactopyranoside at an optical density of 0.8 at 600 nm and the cultures were maintained at 20℃
414 overnight. SARS-CoV2 M^{pro} and C300S M^{pro} were purified first by affinity chromatography using
415 TALON™ cobalt-based affinity Resin (Takara Bio). The His_6-tag was cleaved off by PreScission protease

416 and the resulting authentic 306 amino acid M^{pro} (see Figure S1A in supplemental material) and C300S
417 M^{pro} were further purified by SEC using a HiLoad Superdex 200 pg column (GE Healthcare) in 20 mM
418 Tris, pH 7.5, 150 mM NaCl, and 2 mM DTT. The purity and molecular mass of M^{pro} were assessed by LDS-
419 gel electrophoresis as well as reverse phase high performance liquid chromatography (RP/HPLC) on a C18
420 column coupled with a Matrix-Assisted Laser Desorption/Ionization-Time of Flight (MALDI-TOF) mass
421 spectrometer (MS). The purity of these M^{pro}'s was greater than 95% by LDS-gel electrophoresis, RP-HPLC
422 chromatography (205 nm), and MALDI-TOF analysis (see Figure S1B-S1E in supplemental material), with
423 an average experimental mass of 33796 amu +/- 1 amu (expected average mass of 33796.48 amu) (see
424 Figure S1E and S1I (insets) in supplemental material). Final preparations of M^{pro} (2-6 mg/ml) were stored
425 at -70 in 40 mM Tris-HCl buffer, pH 7.5, 2 mM DTT and 150 mM NaCl.
426
427 ***M^{pro} colorimetric enzyme assay***
428 The enzymatic activity of M^{pro} of SARS-CoV-2 was measured using the custom-synthesized
429 peptide, H2N-TSAVLQ-pNA as described previously [39, 40]. TSAVLQ represents the nsp4↓nsp5 cleavage
430 sequence for SARS and SAS2 M^{pro}. The rate of enzymatic activity was determined by following the increase
431 in absorbance (390 nm) using a Spectramax 190 multiplate reader at 37°C as a function of time following
432 addition of substrate. Assays were conducted in clear flat bottom 96-well plates (Corning) containing 40
433 µL of assay buffer (50 mm Tris, pH 7.5, 2 mM EDTA, and 300 mM NaCl containing 100 ug/ml of cm-
434 BSA). Reactions were started by the addition of 10 µl of 2 mM substrate dissolved in ultrapure water.
435 Activity was obtained by measuring the increase in absorbance at 390 nm as a function of time within the
436 linear range of the assay. A calibration curve was obtained for the product, 4-Nitroanaline (pNA), and was
437 used to convert the rate of the reaction to units of micromoles of product per min per mg of
438 protein(µm/min/mg). In some cases, activity and M^{pro} modifications were determined by first stopping the
439 assay at a set time by acidification with formic acid (FA)/trifluoroacetic acid (TFA) and then analyzed by
440 RP-HPLC using a 2% acetonitrile gradient on a Vydac C18 column as described below. The activity was

441 calculated based on the amount of pNA product (detected at 390 nm). Unprocessed substrate with detected
442 at 320 nm.
443
444 ***Glutathionylation of M^{pro} at pH 7.5 and pH 6.8***
445 To prepare glutathionylated M^{pro} for use in analytical ultracentrifugation, SEC and activity assays,
446 M^{pro} was first exchanged into a buffer containing 40 mM tris-HCL, 2 mM EDTA and 300 mM NaCl at pH
447 7.5 using Amicon 10 kDa cutoff filter units. M^{pro} (1.2-2.2μM as noted in the Results) was then treated only
448 with buffer or with a final of 10 mM GSSG diluted from a stock of 200 mM GSSG that had been adjusted
449 to neutral pH with sodium hydroxide. The solutions were then incubated at 37ºC for 60 min or otherwise
450 as described in the results before removing excess GSSG. Preparations were then diluted 10X with buffer
451 (50 mM tris-HCL, 2 mM EDTA and 100 mM NaCl) and washed 4 times using Amicon 10 kDa cutoff filter
452 units (0.5 ml) to remove excess GSSG. The final preparations were concentrated further with a 0.5 ml 10
453 kDa filtration unit (0.6 mg/ml). In some cases, these preparations were concentrated to 2-6 mg/ml) for use
454 in SEC. While the extent of glutathionylation varied among preparations the procedure usually yielded
455 preparations of M^{pro} that contained predominantly diglutathionylated M^{pro} based on MS deconvolution
456 analysis as well as monoglutathionylated and triglutathionylated forms.
457 To selectively modify M^{pro} with GSSG on the more reactive cysteine residues, a similar procedure
458 to that above was used except 5 mM GSSG was used and we lowered the buffer pH to 6.8. Prior to
459 modification, M^{pro} was treated with 50 mM TCEP for 30 minutes to ensure all cysteines were in their
460 reduced form and then TCEP removed by multiple washes through an Amicon 10 kDa cutoff filter with pH
461 6.8 incubation buffer (50 mM tris-HCL, 2 mM EDTA and 100 mM NaCl). For glutathionylation, M^{pro} (1.2
462 μM) was incubated for 2.5 hours at 37ºC in 50 mM Tris-HCl buffer, 300 mM NaCl, and 2 mM EDTA at
463 pH 6.8 with buffer (control) or 5 mM GSSG. The preparations were then washed 4 times to remove excess
464 GSSG using Amicon 10 kDa cutoff filter units (0.5 ml) with pH 6.8 buffer. This procedure typically resulted
465 in 30-40% of becoming monoglutathionylated with less than 10% diglutathionylated. The percent of the
466 glutathionylated M^{pro} forms was estimated based on the abundances of the different protein forms (obtained

467 by protein deconvolution). Although these forms are similar in molecular weight, they would have
468 somewhat different ionization potentials and therefore the numbers are only an estimate of percent
469 modification.

470 To confirm the identity of certain peptide fragments we purchased synthetic peptides and modified
471 them accordingly and determined their masses and retention times on the RP-HPLC/MS analysis. Peptides
472 (100 μM) corresponding to chymotryptic fragments from digested M^{pro} (113:118, 127:134, 141:150,
473 155:159, 295: 305) were glutathionylated with 10 mM GSSG in 50 mM Tris-HCl buffer, 300 mM NaCl,
474 and 2 mM EDTA pH 7.5 for 1 hour. These same peptides as well as 295: 306 and the tryptic peptide 299:306
475 were alkylated with 5 mM NEM for 30 minutes at 37 ºC then acidified to pH less than 3.0 with formic acid.
476 Glutathionylation and NEM alkylation of the peptides was verified using RP-HPLC/MS TOF analysis on
477 a Vydac C18 column with the same method that was used for analysis of trypsin/lysC and chymotrypsin
478 digests of M^{pro} as described below.

479

480 ***Grx Assays on Glutathionylated forms of M^{pro}***

481 To determine if Grx could deglutathionylate M^{pro}, monoglutathionylated preparations of M^{pro}
482 containing 30-40% monoglutathionylated or multiglutathionylated M^{pro} (prepared as described in
483 "Glutathionylation of M^{pro} at pH 7.5 and pH 6.8") (8 μM) were used. For preparations made at pH 7.5
484 which had predominantly diglutathionylated M^{pro} the preparation was incubated at 37ºC for 30 minutes in
485 the presence of buffer control (50 mM Tris, pH 7.5, 2 mM EDTA, and 100 mM NaCl containing 100 ug/ml
486 of cm-BSA), Grx (350 nM) alone, GSH alone (0.5 mM) and Grx and GSH together. The samples were then
487 analyzed for M^{pro} activity and by SEC3000/MALDI-TOF to assess the different forms of M^{pro}. The eluting
488 protease was analyzed by protein deconvolution (8.3-10 min) to determine the M^{pro} species present. For
489 glutathionylated preparations made at pH 6.8 the M^{pro} was incubated for 15 min at 37°C in 50 mM Tris, pH
490 7.5, 2 mM EDTA, and 100 mM NaCl containing 100 ug/ml of cm-BSA, Grx (88-350 nM), 0.1 mM GSH
491 or 0.1 mM GSH with 88-350 nM Grx in a total volume of 10 μL. After incubation an aliquot of each sample
492 was assayed for M^{pro} activity (1 μM) and analyzed (2 μL) by SEC/MALDI-TOF to determine the percent

493 of glutathionylation in each treatment based on the abundances of each species. For these experiments, the
494 enzyme activity was assessed after stopping the reactions by acidification with FA/TFA and determining
495 the pNA product produced using RP-HPLC, as described above, to quantitate the amount of pNA product
496 generated over the 5 min incubation. TCEP treated glutathionylated enzyme was used to obtain the
497 maximum native M^{pro} activity.
498
499 ***Chymotrypsin and trypsin/lysC digestion and analysis of native and glutathionylated M^{pro}***
500 Native M^{pro} and M^{pro} which was monoglutathionylated (~30%) as described above was digested
501 with chymotrypsin or trypsin/lysC using the Accumap™ low pH sample preparation with urea under
502 nonreducing conditions (Promega). The free cysteines in the M^{pro} preparations (100 µg) were first alkylated
503 with N-ethylmaleimide in 8 M urea for 30 min at 37ºC. Complete alkylation of all cysteines of the native
504 M^{pro} with NEM was verified by RP-HPLC/MS-TOF analysis. For chymotrypsin digestion the alkylated
505 proteins were diluted to 1 M urea with 100 mM Tris and 10 mM CaCl2 buffer pH 8.0 (50 µg of protease in
506 57 µl added to 456 µl of buffer) and treated with 2.5 µg of chymotrypsin made fresh in 1 mM HCl. Samples
507 were incubated overnight (18 hours) at 37ºC before stopping the reactions with a final of 2% TFA to reach
508 a pH of <3.0. For typsin/r-LysC digestions the alkylated proteins were digested with low pH resistant r-
509 Lys-C for 1 hours at 37ºC followed by continued digestion with AccuMAP™ Modified Trypsin and
510 AccuMAP™ Low pH Resistant rLys-C for 3 hours, as described in the AccuMAP™ protocol. The peptide
511 digests were then cleaned up using peptide desalting columns (ThermoFisher) following the manufacturer's
512 instructions. The desalted clarified peptide mixtures were then dried in a Thermo speed vacuum system and
513 resuspended in RP-HPLC solvent A (water with 0.1% FA/0.02%TFA). Aliquots of the peptide digests were
514 then analyzed without or with TCEP-Cl treatment (50 mM) to remove glutathione modifications and then
515 were separated on a Vydac C18 column. For peptide analysis the starting conditions were 100% solvent A
516 (water with 0.1% FA/0.02%TFA). Elution of peptides was done with a 1%/min solvent B (acetonitrile with
517 0.1% FA/0.02%TFA) gradient over the first 20 minutes followed by a 2%/min gradient over the next 10
518 minutes. The elution of peptides was monitored using UV absorbance at 205, 254, and 276 nm as well as

519 MALDI-TOF detection. Peptide digests were analyzed without and with TCEP (for native M^{pro} see Figure
520 S2A and Figure S2B for UV and TIC chromatograms respectively and for monoglutathionylated M^{pro}
521 digests without see Figure S2C and Figure S2D for UV and TIC chromatograms respectively or with TCEP
522 analysis see Figure S2E and Figure S2F for UV and TIC chromatograms respectively). Chymotrypsin
523 digestion of alkylated M^{pro} is predicted to produce 10 alkylated cysteine-containing peptides in addition to
524 12 other non-cysteine containing peptides of 3 amino acids or more. The predicted monoisotopic molecular
525 masses for these peptides and their glutathionylated forms were used to extract specific peptide ions from
526 the TIC chromatograms and the masses found were further confirmed by monoisotopic deconvolution.
527 When glutathionylated masses were found, we then searched for their native counterparts following TCEP
528 reduction. We could locate 6 of the 10 predicted alkylated cysteine containing peptides (covering 7 of the
529 12 cysteines) following chymotrypsin digestion of M^{pro} (see Table S1 for a list of peptides found in
530 supplemental material). In addition to the predicted cysteine containing peptides, based on chymotrypsin
531 digestion, the masses for two other cysteine containing peptides were identified including a 151:159 peptide
532 fragment (containing cys156) and a 305:306 peptide fragment (containing cys300). These were produced,
533 presumably, as a result of incomplete digestion by chymotrypsin at the 154:155 and 305:306 predicted
534 cleavage sites (see Table S1, 7b and 10b, respectively, in supplemental material). We also found molecular
535 masses consistent with 10 other non-cysteine containing peptides generated by chymotrypsin digestion (see
536 Table S1 in supplemental material).

537 Trypsin/lysC digests were analyzed by RP-HPLC/MALDI-TOF for both native (see Figure S4A
538 for TIC chromatogram and S4B for UV chromatogram in supplemental material) and monoglutathionylated
539 preparations before (see Figure S4C for TIC chromatogram and S4D for UV chromatogram in supplemental
540 material) and after TCEP treatment (see Figure S4E for TIC chromatogram and S4F for UV chromatogram
541 in supplemental material). Trypsin/lysC digestion is predicted to yield 7 cysteine-containing peptides and
542 5 of the 7 cysteine alkylated peptides were found by molecular mass extraction from the TIC obtained by
543 RP-HPLC/MALDI-TOF (see Table S2 in supplemental material). In addition to the predicted cysteine
544 containing peptides, the masses for two other cysteine containing peptides were identified including a 41:61

545 peptide, resulting from incomplete cleavage at the 60:61 trypsin cleavage site, and a mass consistent with
546 the tryptic peptide 299:306 having undergone spontaneous formation of the pyroglutamate form of the
547 peptide (see Table S2 in supplemental material). This is commonly seen among peptides with N-terminal
548 glutamates[21] and its retention time and mass were confirmed using a synthetic peptide standard that
549 contained both native and pyroglutamate forms.
550
551 ***RP-HPLC MS-TOF analysis***
552 Samples from the colorimetric enzyme assay, as described above, were analyzed by RP-HPLC with
553 an Agilent 1200 series chromatograph on a Vydac C18-column (218TP5205, Hesperia, CA). Samples were
554 injected (25-45 μL) and pNA substrate, pNA product and native and modified forms of M^{pro} were eluted
555 with a 2%/min acetonitrile gradient beginning with 95% solvent A (0.1% FA)/0.02% TFA) in HPLC/MS
556 grade water and 5% solvent B (0.1% FA/0.02% TFA in acetonitrile). The 2% gradient continued for 30
557 minutes and then was ramped to 95% acetonitrile in 2 minutes followed by a 5-minute re-equilibration to
558 the starting conditions. Elution of samples was monitored at 205 nm, 276 nm, 320 nm (for pNA substrate)
559 and 390 nm (for pNA product) with an Agilent diode array detector followed by MS analysis with an
560 Agilent 6230 time of flight MS configured with Jetstream. M^{pro} and its glutathionylated forms eluted
561 between 24-26 minutes (approximately 57% acetonitrile). The mass of the protein was determined by
562 protein deconvolution using Agilent's Mass Hunter software. The TOF settings were the following: Gas
563 Temperature 350ºC, drying gas 13 L/min, nebulizer 55 psi, sheath gas temperature 350ºC, fragmentor 145
564 V, and skimmer 65 V. The mass determination for peptides was done by deconvolution (resolved isotope)
565 using Agilent Mass Hunter software (Agilent).
566
567 ***Analysis of M^{pro} by SEC coupled with MALDI-TOF MS detection***
568 Size exclusion chromatography (SEC) on native and glutathionylated forms of M^{pro} was carried out
569 using BioSep SEC3000 column and subsequently a BioSep SEC2000 column (300 mm × 4.6 mm;
570 Phenomenex, Torrance, CA, U.S.A.) with 25 mM ammonium formate buffer (pH 8.0) running buffer on a

571 1200 series HPLC–MS system (Agilent, Santa Clara, CA, U.S.A.). The isocratic flow rate was 0.35 ml ·
572 min^{-1} and M^{pro} samples were injected at 2 µl. Where indicated, cm-BSA was used as a carrier to help
573 prevent nonspecific binding of protein during the analysis. Proteins eluting from the column were monitored
574 using an Agilent 1100 series fluorescent detector connected in series with the Agilent 6230 MS-TOF
575 detector. At high concentrations, M^{pro} eluted as a single peak with a tailing edge while at lower
576 concentrations M^{pro} eluted as two peaks consistent with it behaving as a monomer dimer system. For the
577 SEC3000 column the M^{pro} peaks eluted between 8.5-10 minutes while for the SEC2000 column peaks
578 eluted between 7-8.5 minutes. The percent of different forms of M^{pro} was estimated by using the abundances
579 of each species which can only provide an estimate due to variations in ionization potential for each M^{pro}
580 species.
581
582 ***Analytical ultracentrifugation***
583 For analytical ultracentrifugation (AUC) a Beckman Optima XL-I analytical ultracentrifuge, with
584 absorption optics, an An-60 Ti rotor and standard double-sector centerpiece cells was used. Sedimentation
585 equilibrium measurements of authentic native M^{pro} and glutathionylated M^{pro} were used to determine the
586 average molecular weight and dissociation constant (K_d) for dimerization. M^{pro} was diluted into 50 mM Tris
587 pH 7.5 buffer containing 2 mM EDTA and 300 mM NaCl buffer to 1 µM (6 ml total solution) and then was
588 untreated or glutathionylated with 10 mM GSSG for 45 minutes in the same buffer. Both preparations were
589 washed by passing through a 10 kDa cut-off Amicon membrane and washing 4 times with 50 mM tris
590 buffer with 2 mM EDTA and 100 mM NaCl. The preparations were analyzed by RP-HPLC/MS and control
591 contained native M^{pro} while the glutathionylated preparation had predominantly diglutathionylated protease
592 (63%), as well as triglutathionylated protease (22%) and monoglutathionylated protease (15%) based on
593 their relative abundances. There was no detectable native M^{pro} remaining in this glutathionylated
594 preparation. Proteins were concentrated to 0.63 mg/ml in 50 mM tris buffer pH 7.5 with 2 mM EDTA and
595 100 mM NaCl. Samples (100 µl) were centrifuged at 20ºC at 21,000 rpm (16h) and 45,000 (3h) overspeed

596 for baseline. Data (the average of 8 – 10 scans collected using a radial step size of 0.001 cm) were analyzed
597 using the standard Optima XL-I data analysis software v6.03.
598
599 ***Statistical analysis***
600 Statistical analyses were performed using two-tailed Student's *t-test* (paired) on experiments with
601 at least 3 biological replicates or using a two-way ANOVA followed by Šídak's multiple comparison post
602 hoc test. P-values less or equal to 0.05 were considered statistically significant, *<0.05, **<0.01 and
603 ***<0.005.
604
605 **Acknowledgements**
606 This research was supported in part by the Intramural Research Program of the National Institutes of Health,
607 National Cancer Institute and National Institute of Arthritis and Musculoskeletal and Skin Diseases. We
608 thank Rodney Levine (National Heart, Lung and Blood Institute) and John Mieyal (Case Western Reserve
609 University) for helpful discussions during this work.
610
611 **Author Contributions:** Conceptualization, D.A.D. and R.Y.; investigation, D. A. D., H. B., P.S., A.Y., H.
612 J., P.T.W., S.H. and H.M; original draft writing, D.A.D. and R.Y.; writing-review and editing, all authors;
613 Funding acquisition, H.M. and R.Y.
614
615 **Competing interests:** All authors declare no competing interests.
616 **Materials & Correspondence:** address to David A. Davis and/or Robert Yarchoan
617 **Data availability**: All data are available in the main text or the supplementary materials.
618
619
620
621

622

623 **References**

624 1. Jin Z*, et al.* Structure of M(pro) from SARS-CoV-2 and discovery of its inhibitors. *Nature*
625 **582**, 289-293 (2020).
626
627 2. Hattori SI*, et al.* GRL-0920, an Indole Chloropyridinyl Ester, Completely Blocks SARS-
628 CoV-2 Infection. *mBio* **11**, (2020).
629
630 3. Liang PH. Characterization and inhibition of SARS-coronavirus main protease. *Curr Top*
631 *Med Chem* **6**, 361-376 (2006).
632
633 4. Xia B, Kang X. Activation and maturation of SARS-CoV main protease. *Protein Cell* **2**,
634 282-290 (2011).
635
636 5. Anand K, Ziebuhr J, Wadhwani P, Mesters JR, Hilgenfeld R. Coronavirus main proteinase
637 (3CLpro) structure: basis for design of anti-SARS drugs. *Science* **300**, 1763-1767 (2003).
638
639 6. Zhang L*, et al.* Crystal structure of SARS-CoV-2 main protease provides a basis for design
640 of improved alpha-ketoamide inhibitors. *Science* **368**, 409-412 (2020).
641
642 7. Shi J, Sivaraman J, Song J. Mechanism for controlling the dimer-monomer switch and
643 coupling dimerization to catalysis of the severe acute respiratory syndrome coronavirus
644 3C-like protease. *J Virol* **82**, 4620-4629 (2008).
645
646 8. Davis DA*, et al.* Reversible oxidative modification as a mechanism for regulating retroviral
647 protease dimerization and activation. *J Virol* **77**, 3319-3325 (2003).
648
649 9. Davis DA*, et al.* Regulation of HIV-1 protease activity through cysteine modification.
650 *Biochemistry* **35**, 2482-2488 (1996).
651
652 10. Davis DA*, et al.* HIV-2 protease is inactivated after oxidation at the dimer interface and
653 activity can be partly restored with methionine sulphoxide reductase. *Biochem J* **346 Pt 2**,
654 305-311 (2000).
655
656 11. Davis DA, Yusa K, Gillim LA, Newcomb FM, Mitsuya H, Yarchoan R. Conserved
657 cysteines of the human immunodeficiency virus type 1 protease are involved in regulation
658 of polyprotein processing and viral maturation of immature virions. *J Virol* **73**, 1156-1164
659 (1999).
660
661 12. Davis DA, Newcomb FM, Moskovitz J, Fales HM, Levine RL, Yarchoan R. Reversible
662 oxidation of HIV-2 protease. *Methods Enzymol* **348**, 249-259 (2002).
663
664 13. Davis DA, Newcomb FM, Starke DW, Ott DE, Mieyal JJ, Yarchoan R. Thioltransferase
665 (glutaredoxin) is detected within HIV-1 and can regulate the activity of glutathionylated
666 HIV-1 protease in vitro. *J Biol Chem* **272**, 25935-25940 (1997).
667

668 14. Davis DA*, et al.* Analysis and characterization of dimerization inhibition of a multi-drug-
669 resistant human immunodeficiency virus type 1 protease using a novel size-exclusion
670 chromatographic approach. *Biochem J* **419**, 497-506 (2009).
671
672 15. Parker SD, Hunter E. Activation of the Mason-Pfizer monkey virus protease within
673 immature capsids in vitro. *Proc Natl Acad Sci U S A* **98**, 14631-14636 (2001).
674
675 16. Daniels SI*, et al.* The initial step in human immunodeficiency virus type 1 GagProPol
676 processing can be regulated by reversible oxidation. *PLoS One* **5**, e13595 (2010).
677
678 17. Miseta A, Csutora P. Relationship between the occurrence of cysteine in proteins and the
679 complexity of organisms. *Mol Biol Evol* **17**, 1232-1239 (2000).
680
681 18. Huang Z, Pinto JT, Deng H, Richie JP, Jr. Inhibition of caspase-3 activity and activation
682 by protein glutathionylation. *Biochem Pharmacol* **75**, 2234-2244 (2008).
683
684 19. Mieyal JJ, Gallogly MM, Qanungo S, Sabens EA, Shelton MD. Molecular mechanisms
685 and clinical implications of reversible protein S-glutathionylation. *Antioxid Redox Signal*
686 **10**, 1941-1988 (2008).
687
688 20. Checconi P, Limongi D, Baldelli S, Ciriolo MR, Nencioni L, Palamara AT. Role of
689 Glutathionylation in Infection and Inflammation. *Nutrients* **11**, (2019).
690
691 21. Wright HT. Nonenzymatic deamidation of asparaginyl and glutaminyl residues in proteins.
692 *Crit Rev Biochem Mol Biol* **26**, 1-52 (1991).
693
694 22. Cabiscol E, Levine RL. The phosphatase activity of carbonic anhydrase III is reversibly
695 regulated by glutathiolation. *Proc Natl Acad Sci U S A* **93**, 4170-4174 (1996).
696
697 23. Mieyal JJ, Chock PB. Posttranslational modification of cysteine in redox signaling and
698 oxidative stress: Focus on s-glutathionylation. *Antioxid Redox Signal* **16**, 471-475 (2012).
699
700 24. Shelton MD, Mieyal JJ. Regulation by reversible S-glutathionylation: molecular targets
701 implicated in inflammatory diseases. *Mol Cells* **25**, 332-346 (2008).
702
703 25. Naor MM, Jensen JH. Determinants of cysteine pKa values in creatine kinase and alpha1-
704 antitrypsin. *Proteins* **57**, 799-803 (2004).
705
706 26. D'Ettorre C, Levine RL. Reactivity of cysteine-67 of the human immunodeficiency virus-
707 1 protease: studies on a peptide spanning residues 59 to 75. *Arch Biochem Biophys* **313**,
708 71-76 (1994).
709
710 27. Karlstrom AR, Shames BD, Levine RL. Reactivity of cysteine residues in the protease from
711 human immunodeficiency virus: identification of a surface-exposed region which affects
712 enzyme function. *Arch Biochem Biophys* **304**, 163-169 (1993).
713

714 28. Awoonor-Williams E, Rowley CN. Evaluation of Methods for the Calculation of the pKa
715 of Cysteine Residues in Proteins. *J Chem Theory Comput* **12**, 4662-4673 (2016).
716
717 29. Ciriolo MR*, et al.* Loss of GSH, oxidative stress, and decrease of intracellular pH as
718 sequential steps in viral infection. *J Biol Chem* **272**, 2700-2708 (1997).
719
720 30. Luo S, Levine RL. Methionine in proteins defends against oxidative stress. *FASEB J* **23**,
721 464-472 (2009).
722
723 31. Requejo R, Hurd TR, Costa NJ, Murphy MP. Cysteine residues exposed on protein surfaces
724 are the dominant intramitochondrial thiol and may protect against oxidative damage. *FEBS*
725 *J* **277**, 1465-1480 (2010).
726
727 32. Jaimes JA, Andre NM, Chappie JS, Millet JK, Whittaker GR. Phylogenetic Analysis and
728 Structural Modeling of SARS-CoV-2 Spike Protein Reveals an Evolutionary Distinct and
729 Proteolytically Sensitive Activation Loop. *J Mol Biol* **432**, 3309-3325 (2020).
730
731 33. Ge XY*, et al.* Isolation and characterization of a bat SARS-like coronavirus that uses the
732 ACE2 receptor. *Nature* **503**, 535-538 (2013).
733
734 34. Banerjee A, Baker ML, Kulcsar K, Misra V, Plowright R, Mossman K. Novel Insights Into
735 Immune Systems of Bats. *Front Immunol* **11**, 26 (2020).
736
737 35. Wilhelm Filho D, Althoff SL, Dafre AL, Boveris A. Antioxidant defenses, longevity and
738 ecophysiology of South American bats. *Comp Biochem Physiol C Toxicol Pharmacol* **146**,
739 214-220 (2007).
740
741 36. Chionh YT*, et al.* High basal heat-shock protein expression in bats confers resistance to
742 cellular heat/oxidative stress. *Cell Stress Chaperones* **24**, 835-849 (2019).
743
744 37. Costantini D, Lindecke O, Petersons G, Voigt CC. Migratory flight imposes oxidative
745 stress in bats. *Curr Zool* **65**, 147-153 (2019).
746
747 38. Gunther, *et al.* X-ray screening identifies active site and allosteric inhibitors of SARS-
748 CoV-2 main protease. *Science 101126* **science.abf7945**, (2021).
749
750 39. Huang C, Wei P, Fan K, Liu Y, Lai L. 3C-like proteinase from SARS coronavirus catalyzes
751 substrate hydrolysis by a general base mechanism. *Biochemistry* **43**, 4568-4574 (2004).
752
753 40. Wei P*, et al.* The N-terminal octapeptide acts as a dimerization inhibitor of SARS
754 coronavirus 3C-like proteinase. *Biochem Biophys Res Commun* **339**, 865-872 (2006).
755
756 41. DeLano WL. PyMOL molecular viewer: Updates and refinements. *Abstr Pap Am Chem S*
757 **238**, (2009).
758
759

760

Table 1: RP/HPLC/MALDI-TOF MS Identification of peptides from chymotrypsin digestion of monoglutathionylated M^{pro} preparations without (-) and with (+) TCEP

M^{pro} Cys	TCEP	Peptide*	$M_{r\,(calc)}$	$M_{r\,(expt)}$	Delta	RT
Cys156**	-	^{151}NIDYDC^{GSH}VSF^{159}	1379.50	1379.47	0.03	19.0
Cys300	-	^{295}DVVRQC^{GSH}SGVTF^{305}	1514.66	1514.62	0.04	14.9
Cys300***	-	^{295}DVVRQC^{GSH}SGVTFQ^{306}	1642.71	1642.68	0.03	13.6
Cys156**	+	^{151}NIDYDCVSF^{159}	1074.42	1074.41	0.01	20.6
Cys300	+	^{295}DVVRQCSGVTF^{305}	1209.58	1209.56	0.02	16.9
Cys300***	+	^{295}DVVRQCSGVTFQ^{306}	1337.63	1337.61	0.02	15.4

*GSH indicates modification of the cysteine by glutathione based on a monoisotopic mass increase of 305.08. **These peptides containing cysteine 156 occur due to lack of cleavage at the 154:155 predicted chymotryptic cleavage site. *** These peptides containing Cys300 occur due to incomplete cleavage at the 305:306 predicted chymotryptic cleavage site. The retention times (RT) and molecular masses for the Cys300 peptides were confirmed with the use of synthetic peptides that were run on RP-HPLC/MALDI-TOF as native, alkylated or glutathionylated peptides. Peptide samples were analyzed before and after treatment with 50 mM TCEP to remove glutathione moieties. Shown are the calculated native masses [$M_{r\,(calc)}$] and the experimental masses [$M_{r\,(expt)}$] that were obtained from the analysis. The full TIC and 205 nm UV chromatograms for these analyses can be found in supplemental material (see Figure S2C-S2F in supplemental material).

761

762

Table 2: RP/HPLC/MALDI-TOF MS Identification of peptides from trypsin/lysC digestion of monoglutathionylated M^{pro} preparations without (-) and with (+) TCEP

M^{pro} Cys	TCEP	Peptide*	$M_{r\,(calc)}$	$M_{r\,(expt)}$	Delta	RT
Cys85	-	^{77}VIGHSMQNC^{GSH}VLK^{88}	1632.74	1632.71	0.03	13.5
Cys300	-	^{299}QC^{GSH}SGVTFQ^{306}	1173.44	1173.42	0.02	10.9
Cys300**	-	^{299}pyQC^{GSH}SGVTFQ$_{306}$	1156.44	1156.40	0.04	13.6
Cys85	+	^{77}VIGHSMQNCVLK^{88}	1327.66	1327.64	0.02	14.7
Cys300	+	^{299}QCSGVTFQ^{306}	868.36	868.36	0.00	11.2
Cys300**	+	^{299}pyQCSGVTFQ^{306}	851.36	851.33	0.03	14

*GSH indicates modification by glutathione based on a monoisotopic mass increase of 305.08. **These peptides are the result of the spontaneous deamidation that occurs with peptides containing an N-terminal glutamyl residues [21] and the retention times and molecular masses for this peptide were confirmed with the use of synthetic peptides that were run on RP-HPLC/MS. The retention times (RT) and molecular masses for the Cys300 peptides were confirmed with the use of synthetic peptides that were run on RP-HPLC/MALDI-TOF as native, alkylated or glutathionylated peptides. Peptide samples were analyzed without (-) and with (+) TCEP to remove glutathione moieties. Shown are the calculated native masses [$M_{r\,(calc)}$] and the experimental masses [$M_{r\,(expt)}$]. The full TIC and 205 nm UV chromatograms for these analyses can be found in supplemental material (see Figure S5C-S5F in supplemental material).

763

764 **Figure Legends**

765 **Figure 1: Exposure of low concentrations of SARS-CoV-2 M^{pro} to oxidized glutathione results in**
766 **glutathionylation and inhibition of activity.** (A,B) Activity of M^{pro} following a 30-minute pre-incubation
767 of (A) 1.2 μM M^{pro} or (B) 18 μM M^{pro} pretreated with 2 mM or 10 mM oxidized or reduced glutathione.
768 After preincubation, M^{pro} was assayed for protease activity at an equal final enzyme concentration (1 μM).
769 (C,D) M^{pro} molecular masses found by protein deconvolution for M^{pro} eluting off of the C18 reverse phase
770 column following the different treatments at (C) 1.2 μM and (D) 18 μM. The theoretical molecular mass of
771 M^{pro} is 33796.48 and the deconvoluted molecular mass for controls in (C) and (D) was 33797.09 and
772 33,797.34, respectively, as determined using Agilent's Mass Hunter software. The experimental masses are
773 shown above each peak obtained by deconvolution. The native M^{pro} as well as the increases in masses
774 indicative of glutathionylation are indicated for the addition of 1 (+Δ1), 2 (+Δ2), and 3 (+Δ3) glutathione
775 moieties in the deconvolution profiles of GSSG-treated M^{pro}. Observed increases were 304, 609, and 913
776 as compared to the predicted increases of 305.1, 610.2 and 915.3 for addition of 1, 2 or 3 glutathione's,
777 respectively. Based on the abundances, the estimated percent of monoglutathionylation in (C) at 2 mM
778 GSSG was 45% and for 10 mM GSSG there was an estimated 11% mono, 50% di, and 35% tri-
779 glutathionylation, respectively. In (D) after treatment with 2 mM GSSG there was <5%
780 monoglutathionylation and after 10 mM GSSG there was an estimated 34% monoglutathionylation. For
781 (A) and (B) the values shown are the mean and standard deviation for three independent experiments (n=3)
782 while for (C) and (D) the analysis was one time. (*** = p-value < 0.005, paired Students *t-test*). All other
783 comparisons to control activity were not found to be significant p-value >0.05). M^{pro} control activity for (A)
784 was 6.42 +/- 2.5 μM/min/mg and for (B) was 9.6 μM/min/mg, and the percent activity in the treatments is
785 normalized to their respective controls.

786

787 **Figure 2: Inhibition of M^{pro} by glutathionylation can be reversed with reducing agent.** M^{pro} was
788 glutathionylated at pH 7.5 with 10 mM GSSG as described in the Materials and Methods and the extent of
789 glutathionylation was determined by RP/HPLC/MALDI-TOF using a 2% acetonitrile gradient as described

790 in materials and Methods. (A,B) Deconvoluted masses obtained by protein deconvolution of the M^{pro} peak
791 (eluting between 24 and 26 min) for (A) 3 µg (5 µL injection) purified glutathionylated M^{pro} and (B)) 3 µg
792 (5 µL injection) glutathionylated M^{pro} after a 30 min treatment with 10 mM DTT. Shown above each peak
793 is the molecular mass (top number) and the abundance (bottom number) found by protein deconvolution.
794 The native, monoglutathionylated (+Δ1), diglutathionylated (+Δ2), and triglutathionylated (+Δ3) M^{pro}, are
795 indicated in the figures. (C) M^{pro} activity (1 µM final enzyme) for native and glutathionylated M^{pro}
796 preparations after a 30-min incubation in the absence or presence of 10 mM DTT. M^{pro} activity for control
797 in (C) and was 4.95 +/- 1.2 µM/min/mg and percent activity for the different conditions was normalized to
798 their respective controls. The values shown are the average and standard deviation from three separate
799 experiments (n=3) (* = p-value < 0.05, paired students *t-test*, ns = not significant).
800
801 **Figure 3: Size exclusion chromatography and equilibrium analytical ultracentrifugation of M^{pro} and**
802 **glutathionylated M^{pro} indicates glutathionylated M^{pro} behaves as a monomer.** (A,D) M^{pro} and
803 glutathionylated M^{pro} were analyzed by SEC3000/MALDI-TOF. (A) Overlay of the chromatograms for 60
804 µM each of M^{pro} (black line) and glutathionylated M^{pro} (red line) and (D) 7.5 µM each of M^{pro} (black line)
805 and glutathionylated M^{pro} (red line) by monitoring the intrinsic protein fluorescence (excitation 276 nm,
806 emission 350 nm). Glutathionylated M^{pro} was made with 10 mM GSSG at pH 7.5 for 2-2.5 hours as
807 described in Materials and Methods. (C,D) Protein deconvolution profiles for (B) native M^{prov} and (C)
808 glutathionylated M^{pro} that were run as shown in (A). (E,F) Protein deconvolution profile for (E) native M^{pro}
809 and (F) glutathionylated M^{pro} that were run as shown in (D). Shown above each peak are the molecular
810 mass (top number) and the abundance (bottom number) found by protein deconvolution. The earlier eluting
811 peak at 8.5 min is cm-BSA, which was used as a carrier in the runs of M^{pro} to help prevent potential non-
812 specific losses of protein during the run. (G,H) Equilibrium analytical ultracentrifugation of (G) M^{pro} and
813 (H) glutathionylated M^{pro} at 0.63 mg ml^{-1} (18 µM) in 50 mM tris buffer pH 7.5, 2 mM EDTA , and 100 mM
814 NaCl. The absorbance gradients in the centrifuge cell after the sedimentation equilibrium was attained at
815 21,000 rpm are shown in the lower panels. The open circles represent the experimental values, and the solid

816 lines represent the results of fitting to a single ideal species. The best fit for the data shown in (G) yielded
817 a relative molecular weight (*Mr*) of 62,991 +/- 1144 and a K_d for dimerization of 2.4 μM and that shown in
818 (H) yielded a molecular weight of 37,000 +/- 1000 and a K_d for dimerization of 200 μM. The corresponding
819 upper panels show the differences in the fitted and experimental values as a function of radial position
820 (residuals). The residuals of these fits were random, indicating that the single species model is appropriate
821 for the analyses.
822
823 **Figure 4: Size exclusion chromatography of a preparation of monoglutathionylated M^{pro} and analysis**
824 **of M^{pro} activity.** A preparation of M^{pro} containing a mixture of native and monoglutathionylated forms was
825 made by incubating 1.2 μM M^{pro} with 5 mM GSSG for 2.5 hours at 37ºC, at pH 6.8, to increase specific
826 modification of the more reactive cysteines of M^{pro} as described in Materials and Methods. (A) SEC2000
827 elution profile as monitored using the intrinsic protein fluorescence (excitation 276 nm, emission 350 nm)
828 of a 2 μl injection of 8 μM monoglutathionylated M^{pro} preparation and (B) M^{pro} molecular weights found
829 by protein deconvolution of the peaks in (A), (C) Elution profile for the mass of native M^{pro} in the
830 monoglutathionylated preparation and (D) elution profile for the mass of monoglutathionylated M^{pro} in the
831 monoglutathionylated preparation. (E) Elution profile for 2 μl injection of 8 μM monoglutathionylated M^{pro}
832 preparation after treatment with 50 mM TCEP for 15 min. (F) M^{pro} molecular weights found by protein
833 deconvolution after treatment with 50 mM TCEP for 15 min. (G) Elution profile for the mass of native M^{pro}
834 after treatment of monoglutathionylated M^{pro} with 50 mM TCEP for 15 min. (H) M^{pro} activity without (black
835 bars) and with (grey bars) TCEP treatment for peak #1 and Peak #2 from Fig 4A after collecting M^{pro}
836 following SEC of the monoglutathionylated M^{pro} preparation. The values represent the average of 4 separate
837 determinations (n=4) of M^{pro} activity. A two-way ANOVA followed by Šídak's multiple comparison post
838 hoc test was done. P-values less or equal to 0.05 were considered statistically significant, **<0.01 and
839 ***<0.005 (ns= p-value > 0.05).
840

841 **Figure 5: Grx reverses glutathionylation and restores M^{pro} activity.** (A-C) M^{pro} Glutathionylated at pH
842 7.5 was incubated (3 µM final) for 30 min in the presence of (A) buffer control, (B) GSH (0.5 mM) or (C)
843 GSH (0.5 mM) with Grx (final 350 nM). Samples were analyzed by SEC3000/MALDI-TOF and the eluting
844 protease analyzed by protein deconvolution (8.3-10 min) to determine the M^{pro} species present. The
845 experimental masses (top number) are shown as well as the abundances (bottom number) for each peak
846 obtained by deconvolution. The native M^{pro}, as well as the increases in masses indicative of
847 glutathionylation, are indicated for the addition of 1 (+Δ1), 2 (+Δ2), and 3 (+Δ3) glutathione moieties in
848 the deconvolution profiles. (D) Samples of glutathionylated M^{pro} were treated as in (A-C) and then analyzed
849 for M^{pro} activity and compared to unmodified M^{pro}. M^{pro} activity for control in (D) was 5.77+/- 1.5
850 µM/min/mg, and percent activity for the different conditions was normalized to their respective controls.
851 (E-G) Monoglutathionylated M^{pro} was incubated (8 µM final) for 15 min in the presence of (A) buffer
852 control, (B) GSH (0.1 mM) or (C) GSH (0.1 mM) with Grx 350 nM and samples analyzed by
853 SEC2000/MALDI-TOF deconvolution (7.3-8.6 min). (H, I) Samples were prepared as in (E-G) and the
854 percentage of monoglutathionylated M^{pro} and activity was determined after the 15-minute incubation with
855 0, 88, 175, or 350 nm Grx in the presence of 100 µM GSH. (H) Percent of monoglutathionylated Mpro after
856 Grx treatment and (I) M^{pro} activity after Grx treatment. The M^{pro} activity was normalized to the TCEP treated
857 preparation which yielded fully reduced native M^{pro} and was used as 100% activity. For (D) Values
858 represent the average +/- standard deviation of 4 separate experiments (* = p-value < 0.05, ****=p-value
859 < 0.001 paired students t-test, ns=not significant p>0.05). For (H) the values are the average of 3 separate
860 experiments (n=3) and for (I) one experiment performed in duplicate (n=2).
861
862 **Figure 6: Glutathionylation inhibits WT SARS-Cov-2 M^{pro} activity but not C300S M^{pro} activity.** (A)
863 Activity of wild type (WT) and C300S M^{pro} (1 µM enzyme) following a 30-minute pre-incubation of 1.2
864 µM M^{pro} with 10 mM oxidized glutathione. (B) M^{pro} activity for a WT monoglutathionylated M^{pro}
865 preparation (containing approximately 30% monoglutathionylated M^{pro} and 4% diglutathionylated) and a
866 C300S monoglutathionylated M^{pro} preparation (containing approximately 18% monoglutathionylated M^{pro})

867 preincubated for 10 minutes without or with 20 mM DTT. The amount of monoglutathionylated M^{pro} was
868 estimated using the relative abundances of native M^{pro} and glutathionylated M^{pro} following deconvolution
869 of the eluting M^{pro} species from SEC/MALDI-TOF analysis. Values represent the average +/- standard
870 deviation of 3 separate experiments (n=3) (* = p-value < 0.05, ***=p-value < 0.005 paired students t-test,
871 ns=not significant p>0.05).
872
873 **Figure 7: The current model for the regulation of dimerization and activity through reversible**
874 **glutathionylation of M^{pro} and Space filling and close up ribbon model of SARS-CoV-2 M^{pro}. (**A) Model
875 showing that M^{pro} dimer exists in equilibrium with its monomer form with a determine K_d of 2.5 μM. The
876 monomeric M^{pro} is susceptible to glutathionylation at Cys300, and this leads to inhibition of dimerization
877 and loss of activity. Human Grx is able to reverse glutathionylation of Cys300 and restore dimerization and
878 activity. (B) Space filling model of the SARS-CoV-2 M^{pro} dimer (apo form) showing the location of
879 cysteines 156 on the surface and 300 near the dimer interface in the left (pink) protomer (PDB ID 7K3T).
880 (C) Close up ribbon model around Cys300 showing the proximity to protomer 2 (blue) at leucine 141' and
881 the proximity to ASN214, GLN299 and PHE3.
882
883 **Figure 8: The local environment around Cys300 in monomeric SARS-CoV-1 M^{pro}.** Ball and stick
884 model for local environment around cys300 in R298A M^{pro} monomer PDB ID 2QCY (a monomeric form
885 of SARS-CoV M^{pro} mutant R298A at pH 6.0). Structural figures were produced with PyMOL v1.5.0.4 [40].
886
887
888

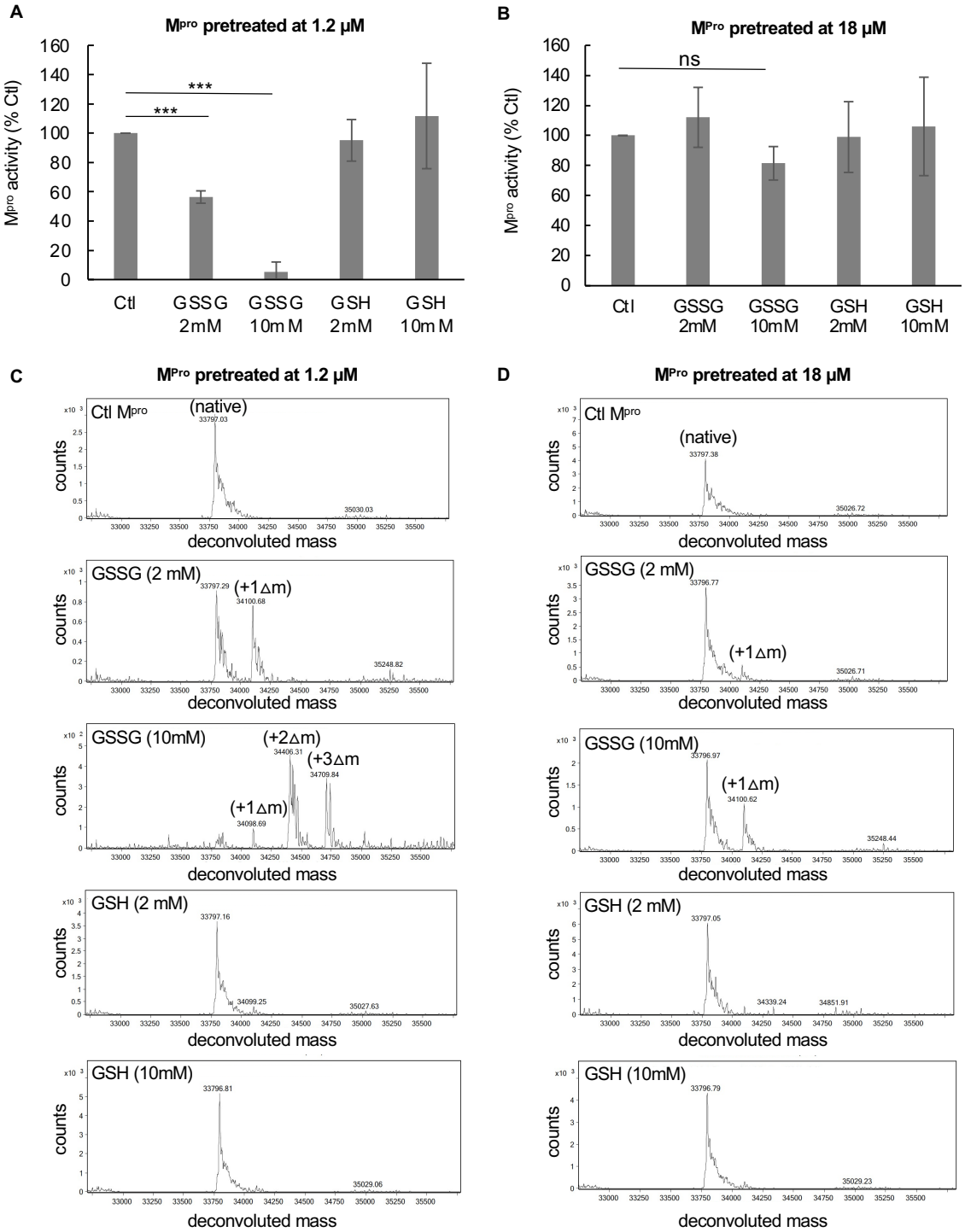

Figure 1: Exposure of low concentrations of SARS-CoV-2 M^{pro} to oxidized glutathione results in glutathionylation and inhibition of activity. (A,B) Activity of M^{pro} following a 30-minute pre-incubation of (A) 1.2 μM M^{pro} or (B) 18 μM M^{pro} pretreated with 2 mM or 10 mM oxidized or reduced glutathione. After preincubation, M^{pro} was assayed for protease activity at an equal final enzyme concentration (1 μM). (C,D) M^{pro} molecular masses found by protein deconvolution for M^{pro} eluting off of the C18 reverse phase column following the different treatments at (C) 1.2 μM and (D) 18 μM. The theoretical molecular mass of M^{pro} is 33796.48 and the deconvoluted molecular mass for controls in (C) and (D) was 33797.09 and 33,797.34, respectively, as determined using Agilent's Mass Hunter software. The experimental masses are shown above each peak obtained by deconvolution. The native M^{pro} as well as the increases in masses indicative of glutathionylation are indicated for the addition of 1 (+Δ1), 2 (+Δ2), and 3 (+Δ3) glutathione moieties in the deconvolution profiles of GSSG-treated M^{pro}. Observed increases were 304, 609, and 913 as compared to the predicted increases of 305.1, 610.2 and 915.3 for addition of 1, 2 or 3 glutathione's, respectively. Based on the abundances, the estimated percent of monoglutathionylation in (C) at 2 mM GSSG was 45% and for 10 mM GSSG there was an estimated 11% mono, 50% di, and 35% tri-glutathionylation, respectively. In (D) after treatment with 2 mM GSSG there was <5% monoglutathionylation and after 10 mM GSSG there was an estimated 34% monoglutathionylation. For (A) and (B) the values shown are the mean and standard deviation for three independent experiments (n=3) while for (C) and (D) the analysis was one time. (*** = p-value < 0.005, paired Students *t-test*). All other comparisons to control activity were not found to be significant p-value >0.05). M^{pro} control activity for (A) was 6.42 +/- 2.5 μM/min/mg and for (B) was 9.6 μM/min/mg, and the percent activity in the treatments is normalized to their respective controls.

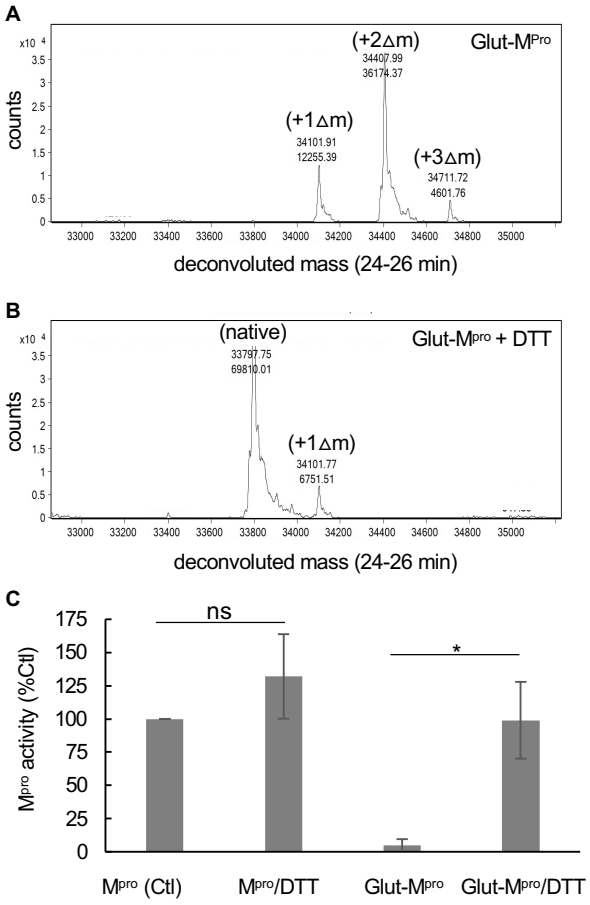

Figure 2: Inhibition of M^{pro} by glutathionylation can be reversed with reducing agent. M^{pro} was glutathionylated at pH 7.5 with 10 mM GSSG as described in the Materials and Methods and the extent of glutathionylation was determined by RP/HPLC/MALDI-TOF using a 2% acetonitrile gradient as described in materials and Methods. (A,B) Deconvoluted masses obtained by protein deconvolution of the M^{pro} peak (eluting between 24 and 26 min) for (A) 3 μg (5 μL injection) purified glutathionylated M^{pro} and (B)) 3 μg (5 μL injection) glutathionylated M^{pro} after a 30 min treatment with 10 mM DTT. Shown above each peak is the molecular mass (top number) and the abundance (bottom number) found by protein deconvolution. The native, monoglutathionylated (+Δ1), diglutathionylated (+Δ2), and triglutathionylated (+Δ3) M^{pro}, are indicated in the figures. (C) M^{pro} activity (1 μM final enzyme) for native and glutathionylated M^{pro} preparations after a 30-min incubation in the absence or presence of 10 mM DTT. M^{pro} activity for control in (C) and was 4.95 +/- 1.2 μM/min/mg and percent activity for the different conditions was normalized to their respective controls. The values shown are the average and standard deviation from three separate experiments (n=3) (* = p-value < 0.05, paired students *t-test*, ns = not significant).

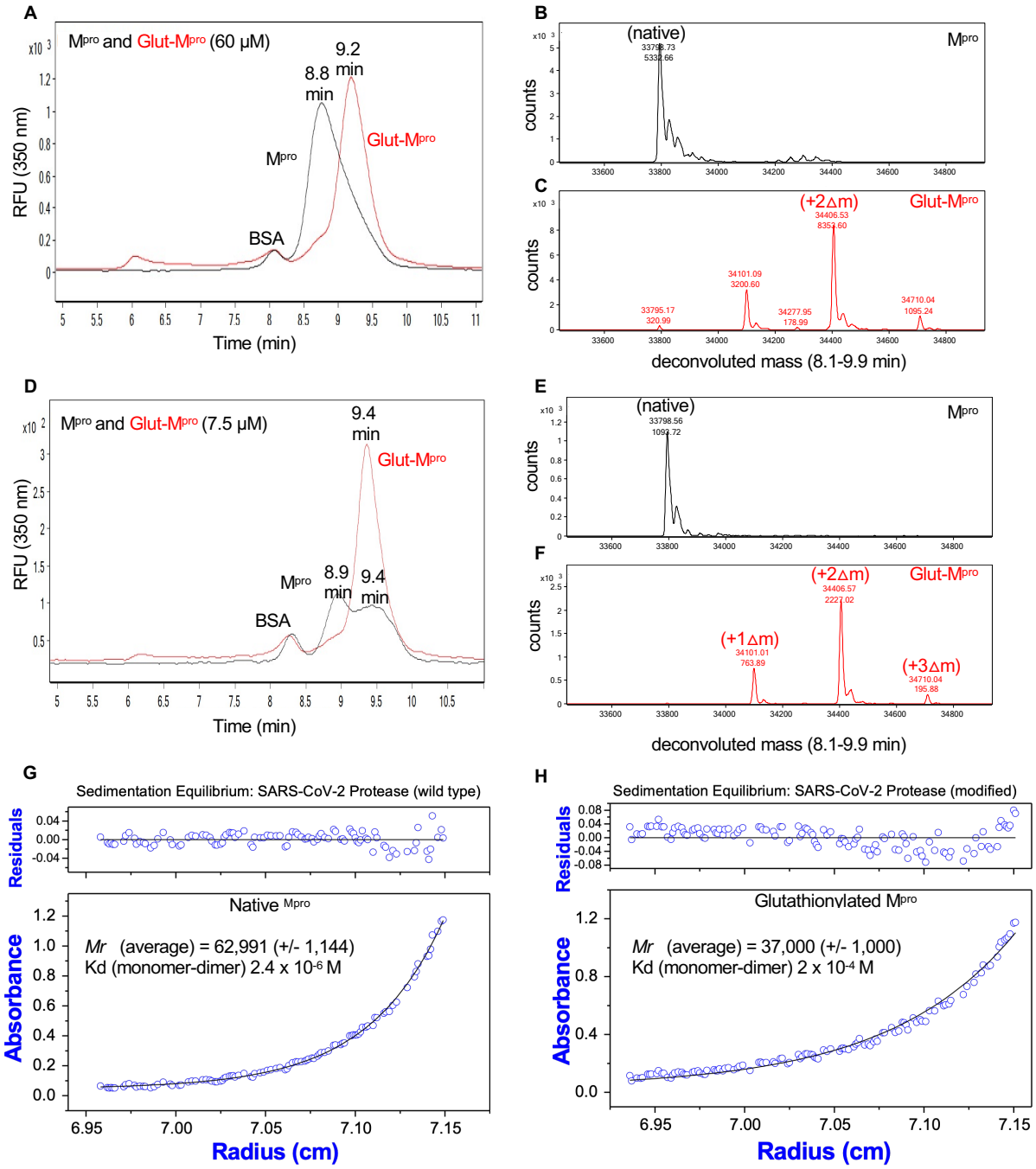

Figure 3: Size exclusion chromatography and equilibrium analytical ultracentrifugation of M^{pro} and glutathionylated M^{pro} indicates glutathionylated M^{pro} behaves as a monomer. (A,D) M^{pro} and glutathionylated M^{pro} were analyzed by SEC3000/MALDI-TOF. (A) Overlay of the chromatograms for 60 μM each of M^{pro} (black line) and glutathionylated M^{pro} (red line) and (D) 7.5 μM each of M^{pro} (black line) and glutathionylated M^{pro} (red line) by monitoring the intrinsic protein fluorescence (excitation 276 nm, emission 350 nm). Glutathionylated M^{pro} was made with 10 mM GSSG at pH 7.5 for 2-2.5 hours as described in Materials and Methods. (C,D) Protein deconvolution profiles for (B) native M^{pro} and (C) glutathionylated M^{pro} that were run as shown in (A). (E,F) Protein deconvolution profile for (E) native M^{pro} and (F) glutathionylated M^{pro} that were run as shown in (D). Shown above each peak are the molecular mass (top number) and the abundance (bottom number) found by protein deconvolution. The earlier eluting peak at 8.5 min is cm-BSA, which was used as a carrier in the runs of M^{pro} to help prevent potential non-specific losses of protein during the run. (G,H) Equilibrium analytical ultracentrifugation of (G) M^{pro} and (H) glutathionylated M^{pro} at 0.63 mg ml^{-1} (18 μM) in 50 mM tris buffer pH 7.5, 2 mM EDTA , and 100 mM NaCl. The absorbance gradients in the centrifuge cell after the sedimentation equilibrium was attained at 21,000 rpm are shown in the lower panels. The open circles represent the experimental values, and the solid lines represent the results of fitting to a single ideal species. The best fit for the data shown in (G) yielded a relative molecular weight (*Mr*) of 62,991 +/- 1144 and a K_d for dimerization of 2.4 μM and that shown in (H) yielded a molecular weight of 37,000 +/- 1000 and a K_d for dimerization of 200 μM. The corresponding upper panels show the differences in the fitted and experimental values as a function of radial position (residuals). The residuals of these fits were random, indicating that the single species model is appropriate for the analyses.

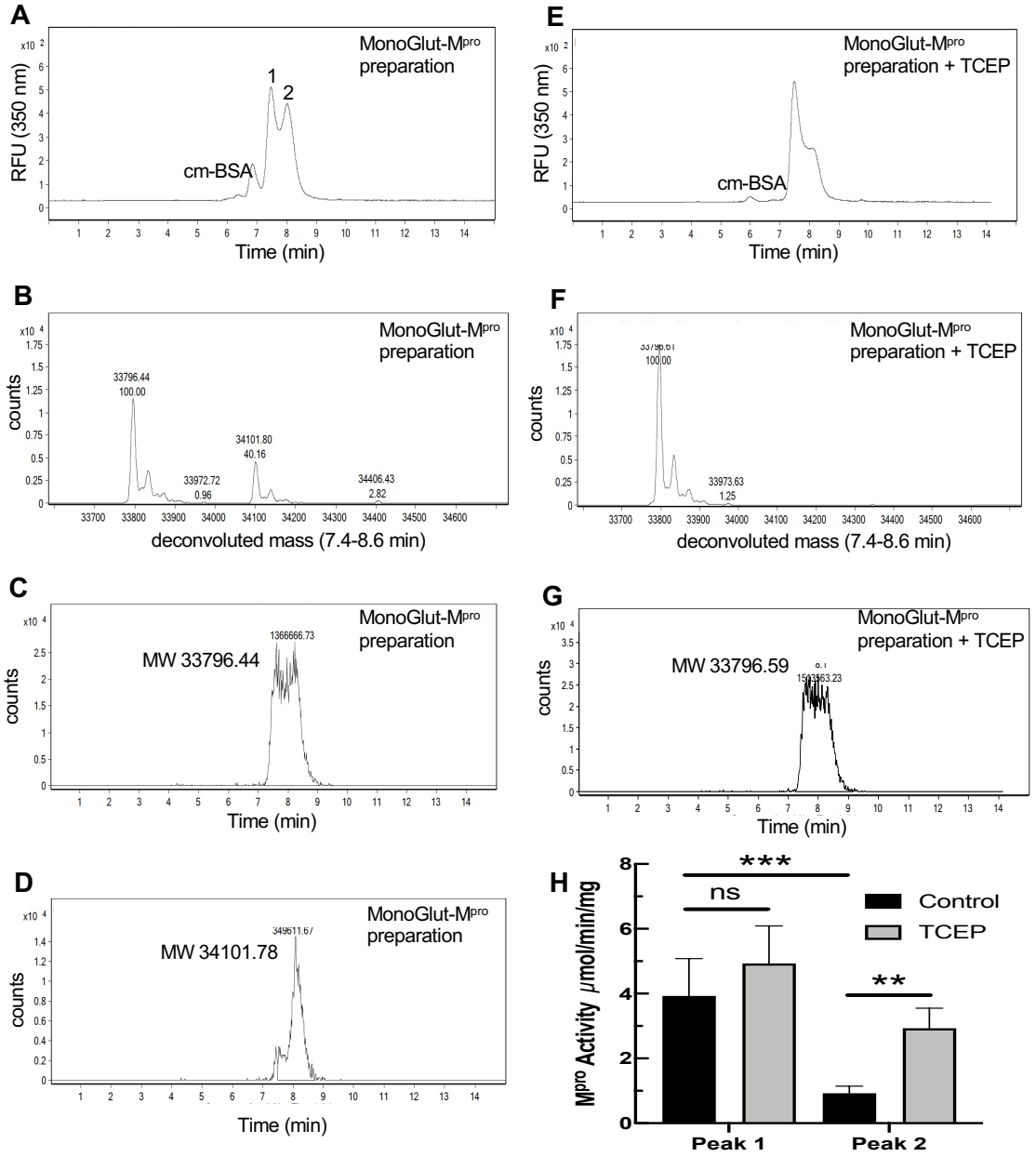

Figure 4: Size exclusion chromatography of a preparation of monoglutathionylated M^{pro} and analysis of M^{pro} activity. A preparation of M^{pro} containing a mixture of native and monoglutathionylated forms was made by incubating 1.2 μM M^{pro} with 5 mM GSSG for 2.5 hours at 37ºC, at pH 6.8, to increase specific modification of the more reactive cysteines of M^{pro} as described in Materials and Methods. (A) SEC2000 elution profile as monitored using the intrinsic protein fluorescence (excitation 276 nm, emission 350 nm) of a 2 μl injection of 8 μM monoglutathionylated M^{pro} preparation and (B) M^{pro} molecular weights found by protein deconvolution of the peaks in (A), (C) Elution profile for the mass of native M^{pro} in the monoglutathionylated preparation and (D) elution profile for the mass of monoglutathionylated M^{pro} in the monoglutathionylated preparation. (E) Elution profile for 2 μl injection of 8 μM monoglutathionylated M^{pro} preparation after treatment with 50 mM TCEP for 15 min. (F) M^{pro} molecular weights found by protein deconvolution after treatment with 50 mM TCEP for 15 min. (G) Elution profile for the mass of native M^{pro} after treatment of monoglutathionylated M^{pro} with 50 mM TCEP for 15 min. (H) M^{pro} activity without (black bars) and with (grey bars) TCEP treatment for peak #1 and Peak #2 from Fig 4A after collecting M^{pro} following SEC of the monoglutathionylated M^{pro} preparation. The values represent the average of 4 separate determinations (n=4) of M^{pro} activity. A two-way ANOVA followed by Šídak's multiple comparison post hoc test was done. P-values less or equal to 0.05 were considered statistically significant, **<0.01 and ***<0.005 (ns= p-value > 0.05).

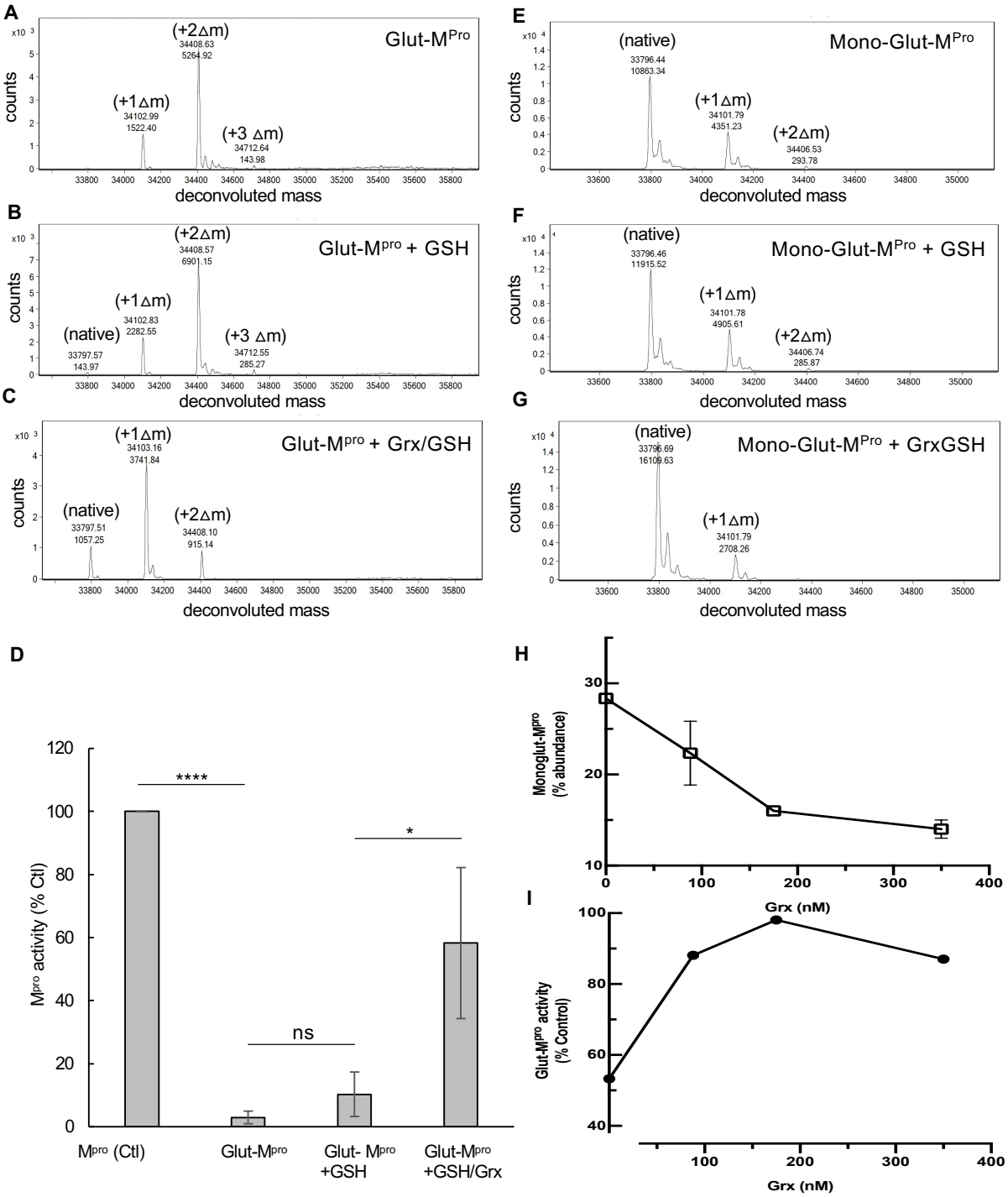

Figure 5: Grx reverses glutathionylation and restores M^{pro} activity. (A-C) M^{pro} Glutathionylated at pH 7.5 was incubated (3 μM final) for 30 min in the presence of (A) buffer control, (B) GSH (0.5 mM) or (C) GSH (0.5 mM) with Grx (final 350 nM). Samples were analyzed by SEC3000/MALDI-TOF and the eluting protease analyzed by protein deconvolution (8.3-10 min) to determine the M^{pro} species present. The experimental masses (top number) are shown as well as the abundances (bottom number) for each peak obtained by deconvolution. The native M^{pro}, as well as the increases in masses indicative of glutathionylation, are indicated for the addition of 1 (+□1), 2 (+□2), and 3 (+□3) glutathione moieties in the deconvolution profiles. (D) Samples of glutathionylated M^{pro} were treated as in (A-C) and then analyzed for M^{pro} activity and compared to unmodified M^{pro}. M^{pro} activity for control in (D) was 5.77+/- 1.5 μM/min/mg, and percent activity for the different conditions was normalized to their respective controls. (E-G) Monoglutathionylated M^{pro} was incubated (8 μM final) for 15 min in the presence of (A) buffer control, (B) GSH (0.1 mM) or (C) GSH (0.1 mM) with Grx 350 nM and samples analyzed by SEC2000/MALDI-TOF deconvolution (7.3-8.6 min). (H, I) Samples were prepared as in (E-G) and the percentage of monoglutathionylated M^{pro} and activity was determined after the 15-minute incubation with 0, 88, 175, or 350 nm Grx in the presence of 100 μM GSH. (H) Percent of monoglutathionylated M^{pro} after Grx treatment and (I) M^{pro} activity after Grx treatment. The M^{pro} activity was normalized to the TCEP treated preparation which yielded fully reduced native M^{pro} and was used as 100% activity. For (D) Values represent the average +/- standard deviation of 4 separate experiments (* = p-value < 0.05, ****=p-value < 0.001 paired students t-test, ns=not significant p>0.05). For (H) the values are the average of 3 separate experiments (n=3) and for (I) one experiment performed in duplicate (n=2).

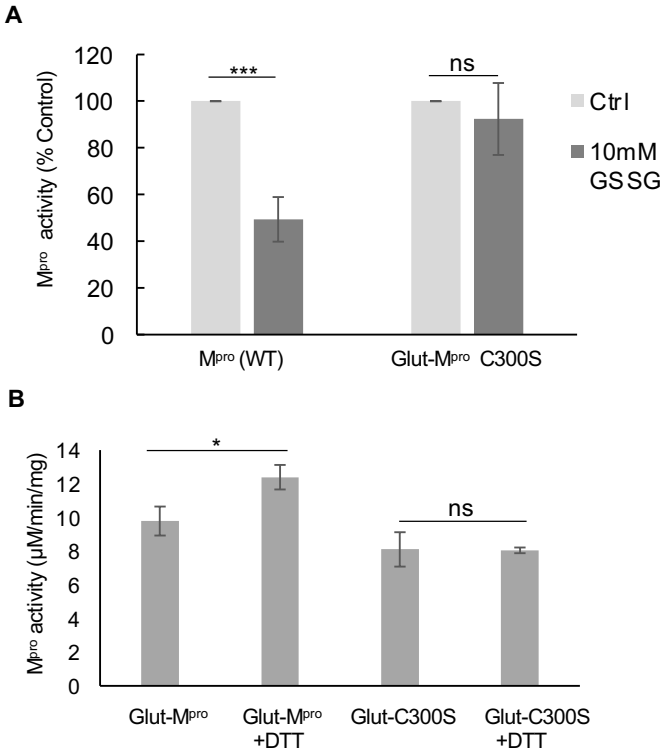

Figure 6: Glutathionylation inhibits WT SARS-Cov-2 M^{pro} activity but not C300S M^{pro} activity. (A) Activity of wild type (WT) and C300S M^{pro} (1 μM enzyme) following a 30-minute pre-incubation of 1.2 μM M^{pro} with 10 mM oxidized glutathione. (B) M^{pro} activity for a WT monoglutathionylated M^{pro} preparation (containing approximately 30% monoglutathionylated M^{pro} and 4% diglutathionylated) and a C300S monoglutathionylated M^{pro} preparation (containing approximately 18% monoglutathionylated M^{pro}) preincubated for 10 minutes without or with 20 mM DTT. The amount of monoglutathionylated M^{pro} was estimated using the relative abundances of native M^{pro} and glutathionylated M^{pro} following deconvolution of the eluting M^{pro} species from SEC/MALDI-TOF analysis. Values represent the average +/- standard deviation of 3 separate experiments (n=3) (* = p-value < 0.05, ***=p-value < 0.005 paired students t-test, ns=not significant p>0.05).

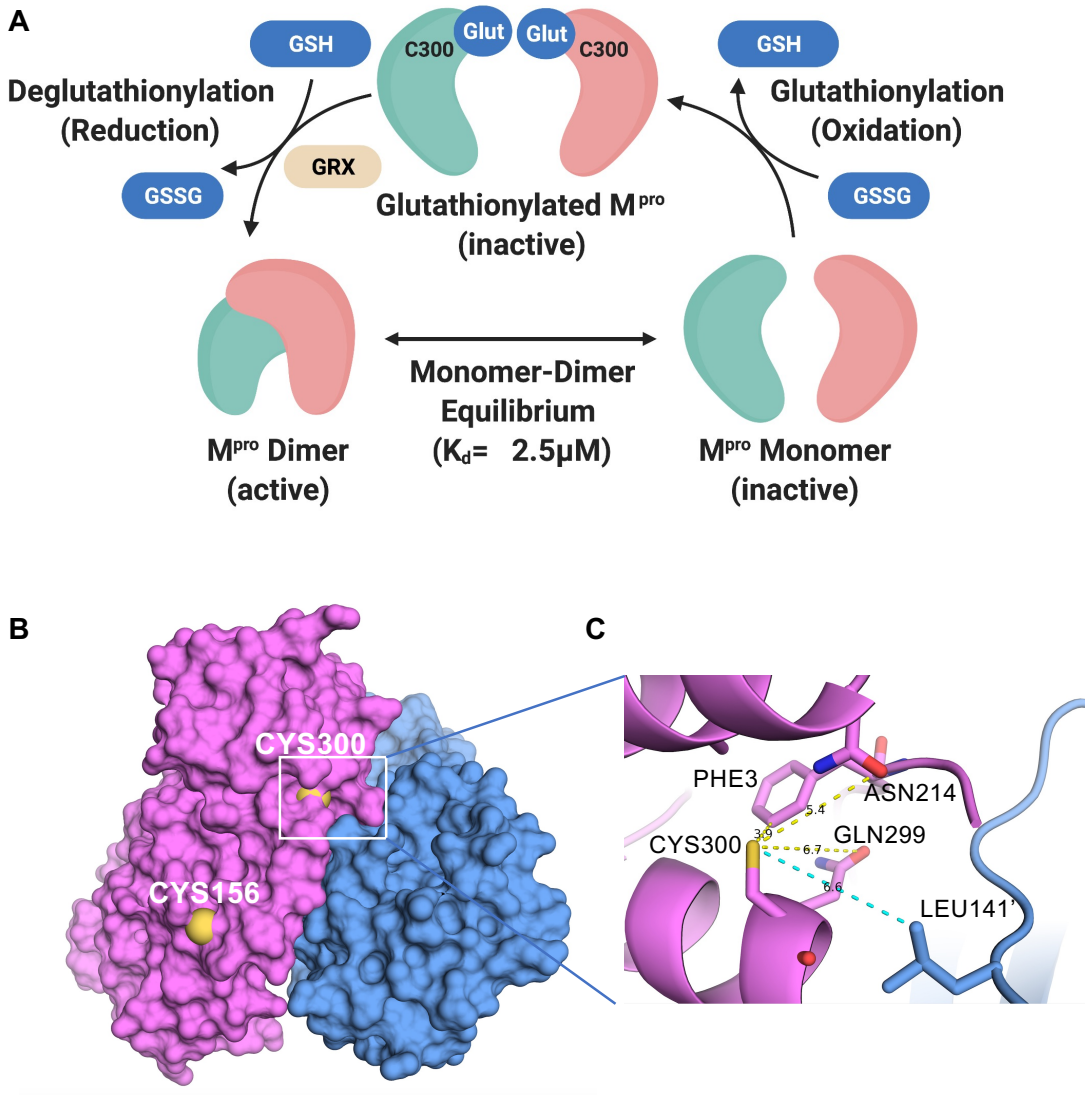

Figure 7: The current model for the regulation of dimerization and activity through reversible glutathionylation of M^{pro} and Space filling and close up ribbon model of SARS-CoV-2 M^{pro}. (A) Model showing that M^{pro} dimer exists in equilibrium with its monomer form with a determine K_d of 2.5 μM. The monomeric M^{pro} is susceptible to glutathionylation at Cys300, and this leads to inhibition of dimerization and loss of activity. Human Grx is able to reverse glutathionylation of Cys300 and restore dimerization and activity. (B) Space filling model of the SARS-CoV-2 M^{pro} dimer (apo form) showing the location of cysteines 156 on the surface and 300 near the dimer interface in the left (pink) protomer (PDB ID 7K3T). (C) Close up ribbon model around Cys300 showing the proximity to protomer 2 (blue) at leucine 141' and the proximity to ASN214, GLN299 and PHE3.

Figure 8

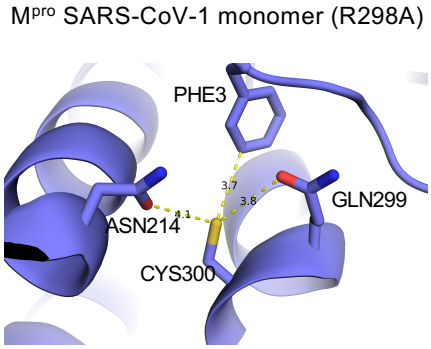

Figure 8: The local environment around Cys300 in monomeric SARS-CoV-1 M^{pro}. Ball and stick model for local environment around cys300 in R298A M^{pro} monomer PDB ID 2QCY (a monomeric form of SARS-CoV M^{pro} mutant R298A at pH 6.0). Structural figures were produced with PyMOL v1.5.0.4 [40].